Title:

Allosteric mechanism of signal transduction in the two-component system histidine kinase PhoQ

Bruk Mensa[1,2,3], Nicholas F. Polizzi[1], Kathleen S. Molnar[4], Andrew M. Natale[1,2,5], Thomas Lemmin[6], William F. DeGrado[1,2]

[1] Department of Pharmaceutical Chemistry, University of California, San Francisco, CA 94158
[2] Cardiovascular Research Institute, University of California, San Francisco, CA 94158, USA
[3] Chemistry and Chemical Biology PhD program, University of California, San Francisco, CA 94158
[4] Codexis Inc., 200 Penobscot Dr, Redwood City, CA 94063, USA
[5] Biophysics PhD program, University of California, San Francisco, CA 94158
[6] Euler Institute, Università della Svizzera italiana, Ch-6900 Lugano, Switzerland

Abstract

Transmembrane signaling proteins couple extracytosolic sensors to cytosolic effectors. Here, we examine how binding of Mg^{2+} to the sensor domain of an *E. coli* two component histidine kinase (HK), PhoQ, modulates its cytoplasmic kinase domain. We use cysteine-crosslinking and reporter-gene assays to simultaneously and independently probe the signaling state of PhoQ's sensor and autokinase domains in a set of over 30 mutants. Strikingly, conservative single-site mutations distant from the sensor or catalytic site strongly influence PhoQ's ligand-sensitivity as well as the magnitude and direction of the signal. Data from 35 mutants are explained by a semi-empirical three-domain model in which the sensor, intervening HAMP, and catalytic domains can adopt kinase-promoting or inhibiting conformations that are in allosteric communication. The catalytic and sensor domains intrinsically favor a constitutively 'kinase-on' conformation, while the HAMP domain favors the 'off' state; when coupled, they create a bistable system responsive to physiological concentrations of Mg^{2+}. Mutations alter signaling by locally modulating domain intrinsic equilibrium constants and interdomain couplings. Our model suggests signals transmit via interdomain allostery rather than propagation

of a single concerted conformational change, explaining the diversity of signaling structural transitions observed in individual HK domains.

Introduction

Two-component system sensor Histidine Kinases (HKs) are conserved signaling modules in bacteria responsible for sensing a myriad of environmental stimuli and orchestrating transcriptional responses along with their cognate transcription factors (Response Regulators, RR) (1, 2). These sensors are generally implicated in environment sensing, and are involved in multi-drug resistance (3–5) and as master regulators of virulence programing in pathogenic bacteria (6, 7). HKs are constitutive homodimers, which transmit signals through a series of intermediary domains to a cytoplasmic catalytic domain. While the lack of a full-length HK structure has hampered our understanding of the mechanism of signal transduction in these proteins, cytoplasmic domain structures have shed light particularly on the enzymatic core of this class of kinases. Several crystallographic snapshots of the autokinase domains of multiple HKs in various conformations (8–14), particularly CpxA, DesK, and VicK, have shown distinct conformations involved in autophosphorylation, phosphotransfer and dephosphorylation that may be conserved across this family. While these structures offer a conserved view of the catalytic cycle of the cytosolic autokinase domain (15), the question of how these proteins couple a sensory event on the other side of the membrane, and many nanometers away to the modulation of the activity of this domain remains unanswered.

This question is especially perplexing in light of the various modular architectures of HKs, involving the insertion of one or more signal transduction domains between sensors and the conserved autokinase domain. It is abundantly clear that the same conserved autokinase domain that defines this protein class can be regulated by a myriad of structural inputs, ranging from

short alpha-helical dimeric coiled coils, to well-folded tertiary folds such as HAMP, PAS and GAF domains (16, 17) (**Figure 1**). Moreover, it is clear from the representation of these folds in diverse protein classes that these domains evolved independently of HKs and were incorporated pervasively into functioning HK architectures. Therefore, they are likely to serve a generalizable function that is robust to evolutionary selection and allow for the construction of physiologically relevant sensors optimally positioned to respond to environmental changes. While some intervening transduction domains have clearly annotated functions, such as the binding of intracellular ligands which are integrated into the sensory function of the HK, the requirement for other signal transduction domains remains obscure.

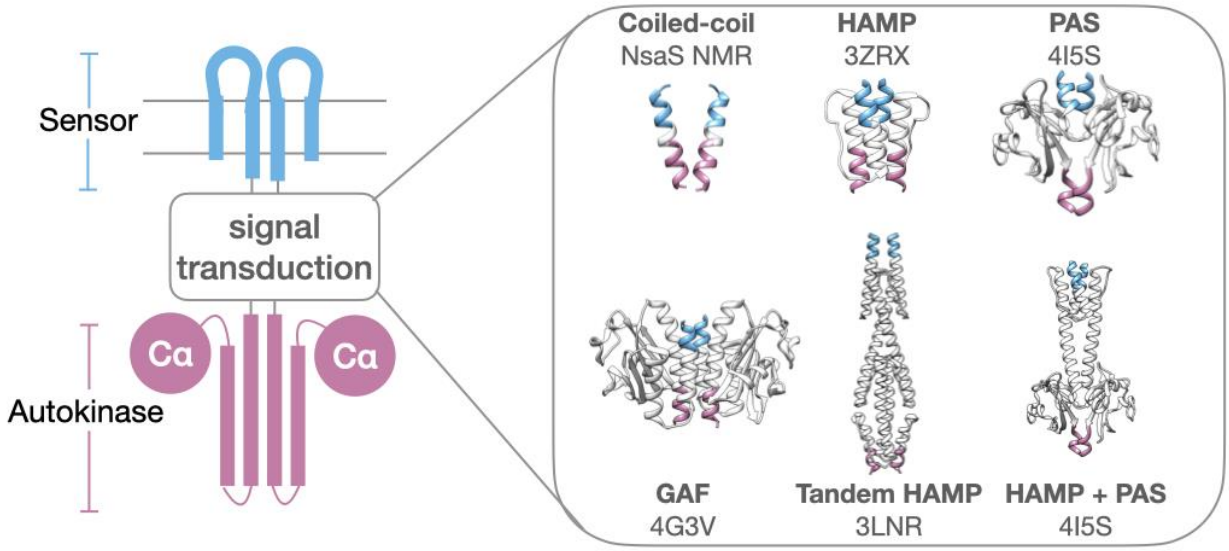

Figure 1 - Modular architecture of histidine kinases. Various protein folds and numbers of signal transduction domains are found inserted between sensor (blue) and autokinase (purple). Structurally elucidated examples include simple coiled-coils (NsaS), HAMP (AF1503), PAS (VicK), GAF (Nlh2), Tandem HAMP (Aer2) and HAMP/PAS domain (VicK). PDB codes are provided in figure, except for NsaS (NMR structure).

In this work, we evaluate the coupling of sensor and autokinase domains in a model Gram-negative HK, PhoQ (18), in which these domains are separated by intervening transmembrane and HAMP signal transduction domains. The PhoQP two-component system is composed of a canonical transmembrane sensor HK, PhoQ, that senses the presence of divalent

cations (19, 20) and polycationic species such as antimicrobial peptides (21, 22), and a cognate response regulator, PhoP (18, 23), which transcriptionally controls regulons related to cation transport and outer-membrane remodeling (24–33). The kinase activity of PhoQ is repressed by divalent cation binding, whereas it is enhanced by the presence of antimicrobial peptides. PhoQ is additionally implicated in low pH sensing (34) via an interaction with the membrane protein UgtL (35), and has more recently been suggested to respond to changes in osmolarity (36). With respect to its most well characterized function, i.e., the sensing of divalent cations such as Mg^{2+}, it is hypothesized that in the absence of such cations, the electrostatic repulsion between an acidic patch in the sensor domain and the negatively charged bacterial inner membrane enforces the 'kinase-on' conformation of the sensor and results in high-kinase/ low-phosphatase activity in the autokinase domain. In the presence of divalent cations, the electrostatic interaction between the sensor and inner-membrane are bridged resulting in a different 'kinase-off' sensor conformation that corresponds to low-kinase/ high-phosphatase autokinase function (37, 38).

To probe the coupling between the sensor and autokinase domains, we established two assays, which allow simultaneous measurement of the conformational states of the sensor and autokinase domains (**Figure 2A**). Like most HKs, PhoQ is a constitutive parallel homodimer, in which the individual domains interact along a series of coaxial helical bundles. Previously, we observed that a Tyr60 to Cys variant forms interchain disulfides between the two monomers only in the absence of Mg^{2+} where the protein is in the 'kinase-on' state (39). Thus, the fraction of the sensor in the 'kinase-on' versus 'kinase-off' state can be readily quantified based on the amount of dimer versus monomer seen in a western blot. Importantly, the Y60C substitution is minimally perturbing, as the [Mg^{2+}]-dependent signaling curve for this mutant is nearly identical to wild type PhoQ with respect to the midpoint of the transition and activity of the basal and activated

states. Also, the redox environment of the periplasm of *E. coli* is buffered such that disulfide formation is reversible and hence a good readout of the conformational state of the sensor (40). To quantify the activity of the auto-kinase domain, we use a well-established beta-galactosidase gene-reporter assay that employs the PhoQ/PhoP-controlled promoter of the Mg^{2+} transporter MgtA. Although this assay is indirect, there is a reasonable correlation between promoter activity and PhoP phosphorylation (41). We note that similar assays, pairing disulfide crosslinking efficiencies to phenotypic output, have been extensively used by Falke, Haselbauer et al. (42, 43) to probe signal transduction in chemosensors that are related to HKs.

Using this approach, we evaluate the extent to which the sensor's conformational state couples to and dictates the conformational activity of the autokinase domain for a set of over 30 mutations, representing substitutions throughout the signal transduction pathway from the sensor to the autokinase domain. We show how these mutations can modulate the three basic characteristics of a PhoQ signaling response which need to fit the biological role of the HK 1) signal strength at limiting high [Mg^{2+}], 2) signal strength at the limiting low [Mg^{2+}], and 3) the midpoint of the [Mg^{2+}] dependent transition – over the physiologically relevant concentration ranges that *E. coli* encounters (0.1- 10 mM). We further evaluate the intrinsic signaling equilibria of the sensor and autokinase domains by disrupting the allosteric coupling between them using poly-glycine insertions in the signal transduction pathway and show that both domains are highly biased to the 'kinase-on' state when uncoupled from each other. The intervening HAMP domain serves as a negative allosteric modulator of both these domains and balances the stability of the 'kinase-on' and 'kinase-off' states so that they can become responsive to physiological concentrations of Mg^{2+}. With these concepts in mind, we establish, fit and evaluate a semi-empirical 3-domain allosteric coupling model to account for the sensor-autokinase coupling and

high/low asymptote and midpoint of transition behaviors of 35 distinct point-mutations and poly-glycine insertions, and highlight the advantages of inserted signal transduction domains in robustly modulating the signaling behavior of HKs.

Results

Single-point mutants along the signal transduction pathway generate a range of sensor and autokinase behavior.

We simultaneously measured the sensor cross-linking and autokinase activities of 'wild type' (Y60C) PhoQ and a total of 35 point mutants and sequence insertions at 5 different concentrations of Mg^{2+} to evaluate the signaling-state correlation of these 2 domains. Our goal was to investigate the mechanism of signal transduction from the sensor to the kinase. To simplify the interpretation of results we maintained wild-type sequences of the Mg^{2+}-binding site and catalytic domain, and mutated at multiple points along the signal transduction pathway. Ala and Phe substitutions were evaluated at sites expected to be on the interior of the protein; these mutants were expected to alter the relative energetics of the kinase- versus phosphatase-promoting states by altering core packing geometry (44–47). We also examined the effects of Trp substitutions in the TM helix at positions expected to map to the headgroup region of the bilayer, as similar substitutions often induce changes in signaling (48–54). We also included several mutations, particularly in the C-terminal half of the HAMP domain, that show altered

autokinase activity as compared to WT PhoQ.

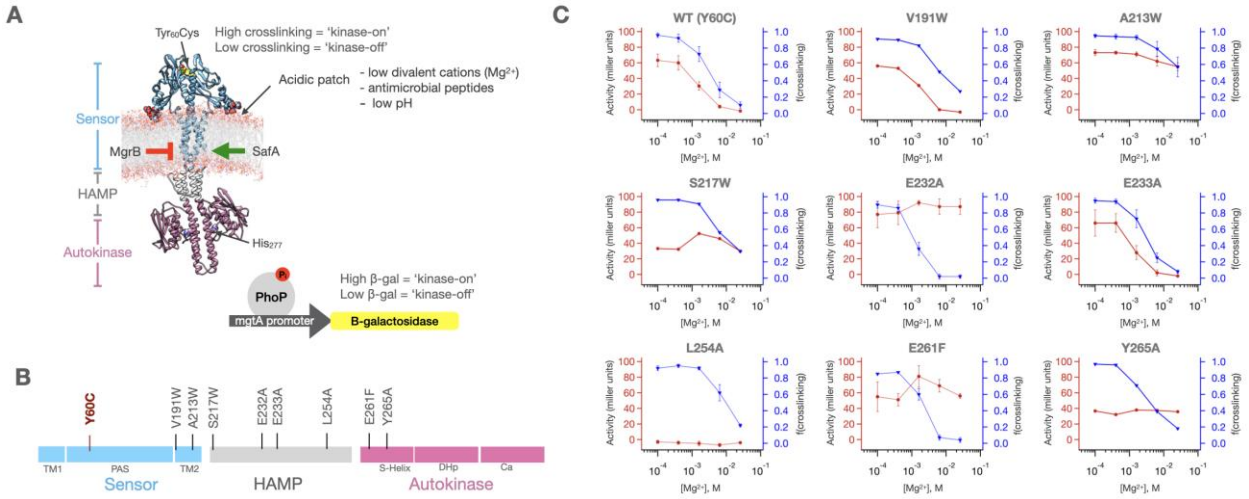

Figure 2 – PhoQ single mutants exhibit a range of behaviors. A) Molecular Dynamics model of dimeric PhoQ in which the sensor (res. 1-219, blue), HAMP (res. 220-260, grey) and autokinase domains (res 261-494, purple) are annotated. The sensor contains a Y60C mutation (spheres) which shows signal state dependent crosslinking. The autokinase contains the conserved catalytic His277, which upon phosphorylation transfers a phosphoryl group to the response regulator PhoP, which then modulates a *mgtA* promoter-driven β-galactosidase reporter. Stimuli and regulatory proteins that modulate PhoQ activity are shown. **B)** Linear topology diagram of PhoQ. The sensor, HAMP and Autokinase domains are highlighted in blue, grey and purple respectively. The locations of mutations in panel **C** are shown. **C)** fraction of sensor crosslinking (blue) and autokinase activity (red) determined for 'wild type' (Y60C) PhoQ, as well as eight mutants along the signal transduction pathway (n=9 for WT, n=2 for A213W, E232A, E233A, L254A and E261F, n=1 for V191W, S217W and Y265A). The sensor state and autokinase activity do not show identical ligand-dependent behavior as would be predicted by a concerted signaling mechanism. Error bars correspond to ±SD, where applicable.

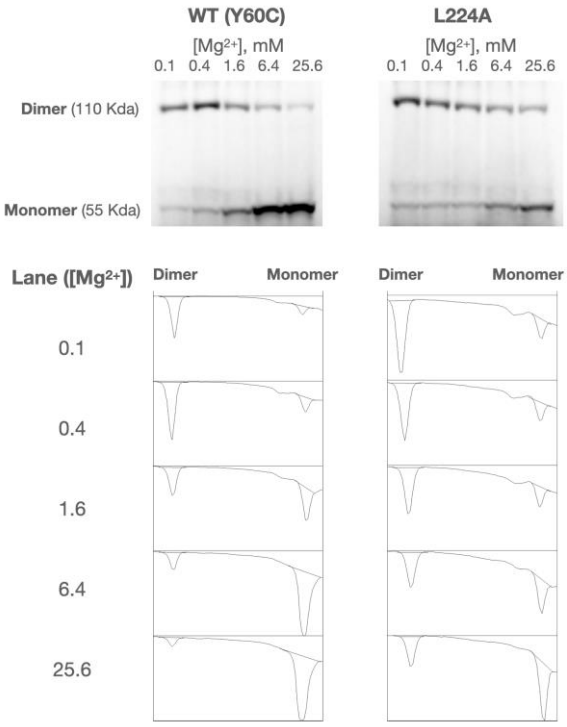

Figure 2-figure supplement 1 – representative PhoQ crosslinking western blot and quantification of WT (Y60C) and Y60C/L224A mutant. LDS buffer solubilized membrane samples are separated by SDS-PAGE and western blotted using an anti-pentaHis antibody. Relative amounts of dimeric and monomeric PhoQ are measured to generate a crosslinking efficiency between 0 and 1.

Illustrative data in **Figure 2C** show it is possible to generate several combinations of ligand-dependent sensor and autokinase behavior. WT (Y60C) PhoQ had a correlated ligand-dependent response, with the high cross-linking state of the sensor corresponding to high autokinase activity at low [Mg^{2+}], and the low cross-linking sensor state corresponding to low autokinase activity at high [Mg^{2+}] (**Figure 2C**). Some mutants however showed low levels of kinase-activity at low [Mg^{2+}] even though the sensor remains in a high-crosslinking 'kinase-on' state (e.g. L254A). Similarly, some mutants retained high kinase-activity in the autokinase despite the fact that crosslinking in the sensor showed WT-like crosslinking in a [Mg^{2+}]-dependent manner (e.g. E232A, E261F). Finally, some mutants produced higher levels of kinase activity at low-Mg^{2+} than WT PhoQ (e.g. E232A is more active than WT PhoQ at low [Mg^{2+}]). Therefore, mutations along the signal transduction pathway have profound effects in altering or uncoupling sensor-autokinase correlation.

The effect of decoupling the HAMP domain from the catalytic and sensor domains.

We examined the intrinsic activities of the sensor and autokinase domains when decoupled from the HAMP domain, by inserting a stretch of 7 helix-disrupting glycines (Gly_7) to interrupt the helical connections that are required for coupling between PhoQ's domains. Gly_7 insertions were introduced just before the HAMP domain (Gly_7 -219/220) as the TM helix exits the membrane and just after the HAMP signal transduction domain within a short helical connection to the autokinase domain (Gly_7 -260/261).

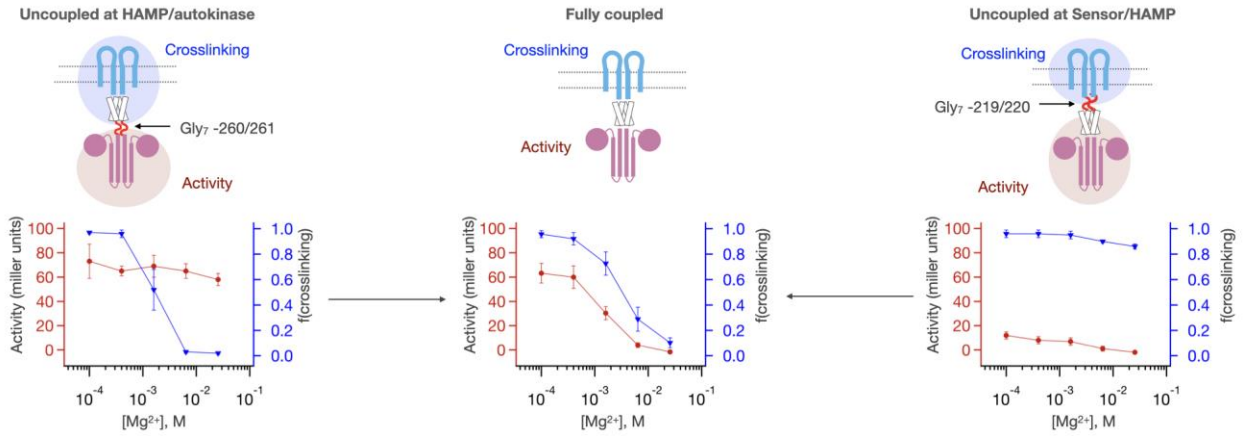

Figure 3 – Intrinsic activities of the PhoQ sensor and autokinase domains are altered by coupling to HAMP. Gly_7 insertions are introduced either between the HAMP domain and the autokinase (Gly_7 - 260/261, left, n=3) or between the Sensor and HAMP domain (Gly_7 -219/220, right, n=2) to disrupt allosteric coupling between sensor and autokinase. Both the sensor and autokinase by themselves show high 'kinase-on' propensity (red trace, left; blue trace, right). The HAMP domain potentiates the 'kinase-off' state, resulting in a more [Mg^{2+}] responsive sensor (blue trace, left), or a lower basal activity autokinase (red trace, right). The fully coupled protein shows correlated sensor/autokinase activity(red and blue traces, middle, n=9).

As expected, both insertions decoupled Mg^{2+} binding from kinase activity (**Figure 3**). However, they had markedly different effects on the sensor and catalytic domains when these activities are evaluated individually. When the insertion occured between the HAMP and sensor domains, the sensor was highly activated, and remained in the high-crosslinking state, even at concentrations of Mg^{2+} sufficient to switch WT PhoQ to the 'kinase-off' state (**Figure 3**, right). On the other hand, if the HAMP domain remained coupled to the sensor, as in WT or the variant with Gly_7 insertion between the HAMP and the catalytic domain (Gly_7 -259/260), the sensor

behaved normally, being efficiently crosslinked in a [Mg^{2+}]-dependent manner (**Figure 3**, left). Thus, the HAMP domain would appear to favor the 'kinase-off' state, serving to reset the energetics of the otherwise highly stable 'kinase-on' state of the sensor.

The HAMP domain had a similar influence on the catalytic domain. When the native connection between the HAMP and the autokinase was disrupted by Gly_7 insertion, the autokinase was highly activated (**Figure 3**, right). By contrast, when the connection between the HAMP and catalytic domains was retained as in Gly_7 -219/220, the kinase activity was strongly downregulated (**Figure 3**, left). Thus, the resulting coupling provides an energetic balance so the system can respond to Mg^{2+} over the physiological range.

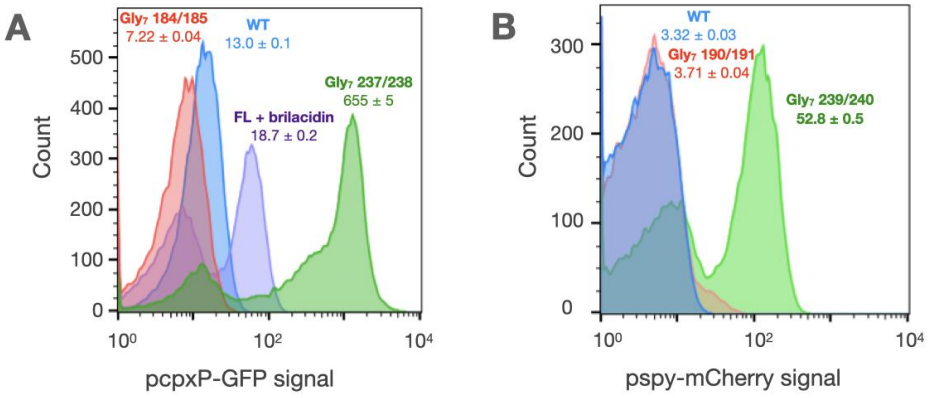

Figure 4 – Glycine disconnections in CpxA and BaeS. A) The activity of CpxA constructs is measured in AFS51 strain (Δ*cpxA*) using a p*cpxP*::GFP reporter. The activity of WT CpxA (blue) is responsive to the antimicrobial mimetic, brilacidin (55, 56) (purple). The autokinase domain of CpxA when uncoupled (Gly_7 237/238) shows very high kinase activity (green), which is repressed to basal levels by the addition of the HAMP domain alone (Gly_7 184/185, red). **B)** The activity of BaeS constructs is measured in a Δ*baeS* Δ*cpxA* strain using a p*spy*::mCherry reporter. The autokinase domain of BaeS when uncoupled shows high kinase activity (Gly_7 239/240, green) relative to WT (blue), which is repressed by the addition of the HAMP domain alone (Gly_7 190/191, red). Median reporter fluorescence values ± STE (n=20,000) are reported below labels for single experiment.

The HAMP domain is negatively coupled to the autokinase domains of CpxA and BaeS

Given the profound effect of the HAMP domain on the intrinsic activities of the PhoQ sensor and autokinase domains, we examined if HAMP domains have similar effects in closely related but functionally distinct HKs with the same arrangement of signaling domains as in PhoQ (TM1, PAS sensor, TM2, a single cytosolic HAMP, and the autokinase domains, **Figure 2A, B**).

We constructed Gly_7 insertions in two closely related *E. coli* HKs, CpxA and BaeS, that have very similar architectures to PhoQ. The HK CpxA responds to periplasmic protein misfolding stress via an accessory protein, CpxP, and upregulates genes to mitigate this stress (57–59). It is similar to PhoQ in that the free HK is kinase-active, and is turned off by the binding of the periplasmic CpxP protein (60). BaeS is a closely related HK, which has significant overlap with CpxA, both in the inducing stimuli as well as the genes regulated (61). We evaluated the activity of these kinases using previously validated fluorescent gene-reporters (p*cpxP*::GFP for CpxA activity(62), p*spy*::mCherry for BaeS activity(56)) in a double CpxA/BaeS knockout strain.

When Gly_7 was inserted immediately upstream of the autokinase domain, we observed a high basal activity for both kinases similar to PhoQ (**Figure 4**). However, when the Gly_7 motif was placed upstream of the HAMP domain thereby allowing to couple to the autokinase, this high basal activity was potently repressed, again similar to PhoQ. This finding indicates that the HAMP domain strongly coupling to and altering the intrinsic activities of adjacent domains may be a generalizable principle, although it might not serve as a negative element in all cases.

Fully cooperative and two-domain allosteric models are unable to explain the gamut of activities of mutants

In the following sections, we consider thermodynamic two-state allosteric signaling models of increasing complexity to understand the coupling of the sensor to the autokinase of WT PhoQ and our set of point-mutants. In these models, we assume that Mg^{2+} binds to single sites in the sensor domains. It is possible that binding between the sites is cooperative or that more than one Mg^{2+} ions are bound per domain. However, given the fact that the transcriptional assay is an indirect readout of the ‘kinase-on’ state, and as such is not necessarily perfectly linear with respect to the fraction of activation (41), we are unable to differentiate between models that

differ subtly in their dose-response curves. However, our data (see below) are able to rule out highly cooperative models in which many binding sites must be occupied with high cooperativity as this would result in a much sharper dose-response curve (63). We also assume that Mg^{2+} can bind to both 'sensor-off' and 'sensor-on' states, albeit with higher affinity to the 'sensor-off' state, as high [Mg^{2+}] inhibits PhoQ kinase activity. Indeed, for the sensor of PhoQ, there is no reason to preclude ligand binding in either sensor state, since the same negatively charged surfaces are present in both states and can conceivably still bind Mg^{2+}, albeit at a much lower affinity due to the lack of bridging interactions (64). Therefore, our model allows for independent Mg^{2+} binding per monomer subunit with built-in stoichiometry factor of 2 in the observed Kds (K_{dOFF}, K_{dON}), but does not consider similar hybrid activation states in the autokinase.

The simplest model for signaling in HKs is one in which the entire HK exists as one concerted domain in a two-state equilibrium of 'kinase-on' and 'kinase-off' states (equilibrium constant = K) which is then modulated by ligand binding (**Figure 5A**). In such a model, PhoQ will be pushed to a fully ligand bound, 'kinase-off' state at high enough [Mg^{2+}] ([Mg^{2+}] >> K_d). At low [Mg^{2+}], the activity of PhoQ is determined by the partition of PhoQ into the low and high affinity Mg^{2+} bound states according to the ratio of the two dissociation constants, K_{dOFF} versus K_{dON}. The midpoint of transition is dictated by the relative magnitudes of K, which reflects PhoQ's preference for the 'kinase-on' vs. 'kinase-off' state, as well as the two K_ds, as shown in **Figure 5A**. However, this model cannot explain why several mutants of PhoQ do not show a 1-to-1 correlation between their sensor and autokinase signaling states (**Figure 2C)**. Moreover, some mutants also have higher autokinase activity than WT PhoQ at low [Mg^{2+}], demonstrating that even at the low-[Mg^{2+}] conditions in which the sensor is fully in the crosslinked 'kinase-on'

state, there remains a significant fraction of the WT autokinase that remains in the 'kinase-off' state. Therefore, this fully concerted signaling model is insufficient to describe the full range of activities of PhoQ variants.

The next model we considered is one in which two domains, sensor and autokinase exhibit two-state equilibria and communicate allosterically. A ligand-dependent sensor can be allosterically coupled to an autokinase domain with a tunable coupling strength to allow for the desired degree of communication between the sensor and the autokinase. In such a scheme, the sensor would be a ligand-binding domain with all the properties previously described for a fully concerted HK. The autokinase on its own would have a constant activity level based on its own intrinsic 'kinase-off' to 'kinase-on' equilibrium. The sensor is then connected to the autokinase in a manner that biases the intrinsic autokinase equilibrium differently depending on which signaling state the sensor is in. A ligand-dependent allosterically modulated HK results from such a coupling, so long as sensor 'kinase-on' and 'kinase-off' states of the sensor alter the autokinase equilibrium differently (**Figure 5B, C**).

To reduce the number of parameters needed to describe such a model, we can define the intrinsic equilibria of the sensor and autokinase when they are connected to a reference state (e.g., 'kinase-off') with equilibrium constants as shown in **Figure 5B**. K_{Sen} is the 'intrinsic' equilibrium of the sensor domain when connected to an autokinase in the 'kinase-off' state, and K_{AK} is the 'intrinsic' equilibrium of the autokinase domain when connected to the sensor in the 'kinase-off' state. When coupled to the 'kinase-on' state of either domain, K_{Sen} and K_{AK} are scaled by a new factor, α. **Figure 5C, 5D** illustrate the effect of α on the Mg^{2+} dose-response curves. When $\alpha = 1$, the two domains are fully uncoupled, and the binding of Mg^{2+} to the sensor is unable to affect the autokinase domain (**Figure 5C**). A value of $\alpha>1$ means that when either of

the domains switches to the 'kinase-on' state, the other domain's propensity to switch 'kinase-on' state is also enhanced by that factor, creating a correlated ligand-mediated transition between sensor and autokinase (**Figure 5D**). If 0<α<1, then a transition to 'kinase-on' state is actually easier when the other domain is in the 'kinase-off' state, creating an anticorrelated ligand dependent behavior. When the absolute value of the log of α becomes very large (i.e., when α is either >>1 or approaching zero), the two domains are highly coupled (**Figure 5D**) and the system behaves as in the fully concerted 2-state models in **Figure 5A**. Therefore, α is the coupling strength between the 'kinase-on' states relative to the coupling strength between the 'kinase-off' states already accounted for in K_{Sen} and K_{AK}.

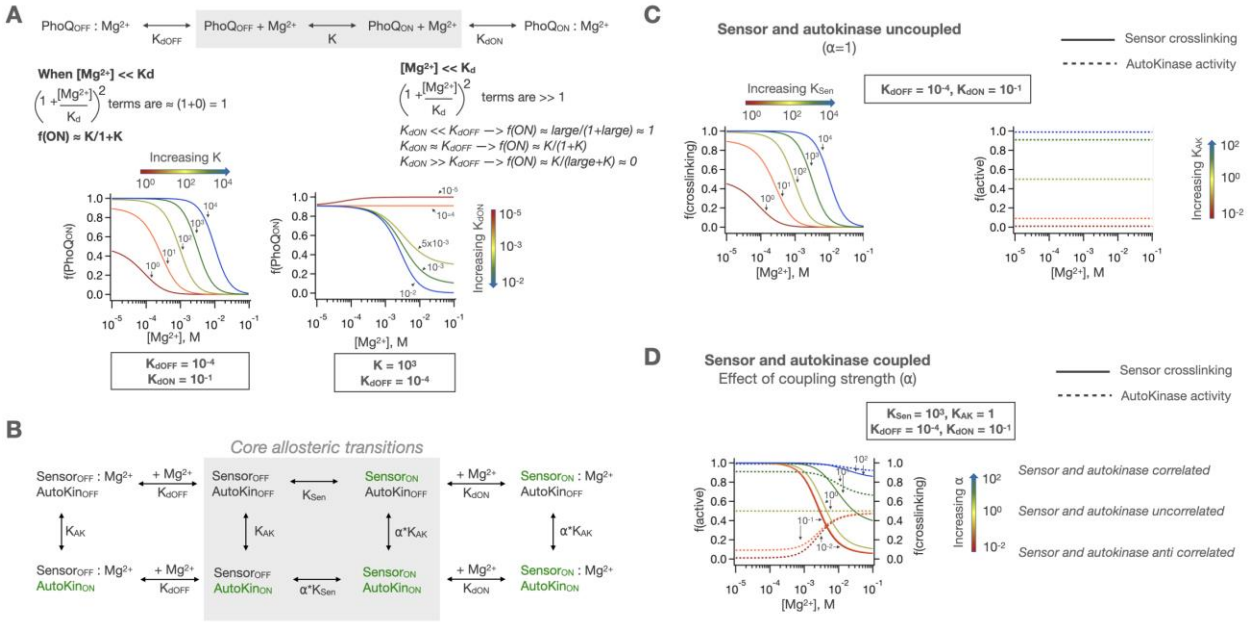

Figure 5 – Concerted and two-domain allosteric models for PhoQ signaling. A) In a concerted model for signaling, PhoQ has an intrinsic on-off equilibrium (constant = K) which is modulated by Mg^{2+} binding to either states with corresponding K_ds. This allows for modulation of both low and high activity asymptotes and the midpoint of transition but requires perfect correlation between sensor and autokinase signaling states. Equations for calculating population fractions are shown in Methods (Equation 1). **B)** The sensor and autokinase domains of PhoQ are allowed to sample both 'kinase-on' and 'kinase-off' states with equilibrium constants K_{Sen} and K_{AK} when the other domain is in the 'kinase-off' state. When the other domain is in the 'kinase-on' state, the equilibria are scaled by the coupling constant, α. This allows for semi-independent fractions of sensor and autokinase in the 'kinase-on' state, which are computed as shown in Methods (Equation 2). **C)** In the uncoupled case (α=1), K_{Sen} modulates the sensor identically to the previously described concerted signaling mechanism, while K_{AK} sets the basal autokinase activity. **D)** The coupling of these domains with α≠1 results in $[Mg^{2+}]$ dependent activity that is either correlated (α>1) or anticorrelated (α<1). As α gets larger, the two domains act more as one concerted protein.

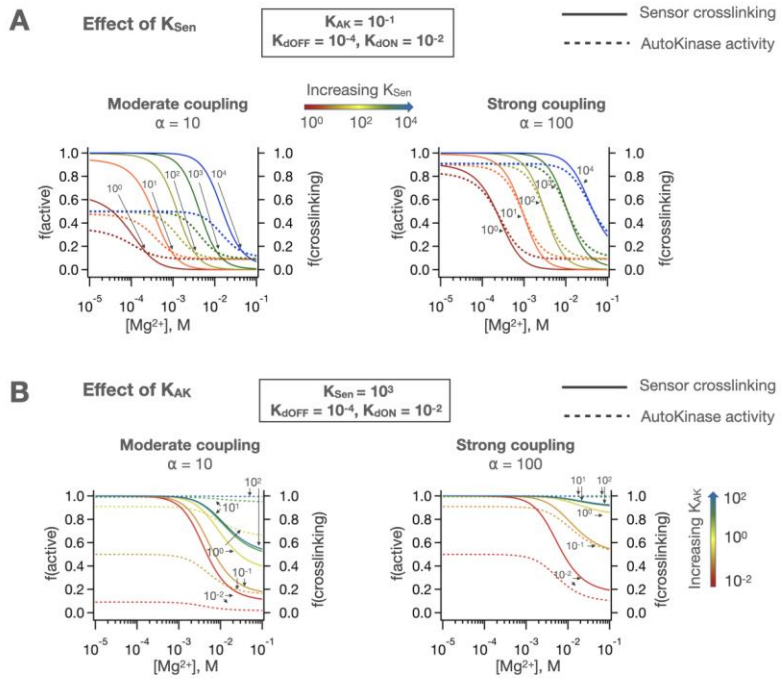

Figure 5-figure supplement 1 – Effects of K_{Sen} and K_{AK} on two-domain signaling. A) Changes in the intrinsic equilibrium of the sensor affect autokinase activity through coupling, and similarly **B)** changes in the intrinsic equilibrium of the autokinase domain can alter the ligand-dependent crosslinking behavior of the sensor.

Coupling provides a robust mechanism for setting both the upper and lower activity asymptotes of the WT sensor kinase. At high enough [Mg^{2+}], the low-crosslinking 'kinase-off' state of the sensor becomes dominant, and the corresponding activity of the autokinase will be dictated by the autokinase equilibrium when coupled to this 'kinase-off' state, K_{AK}. At low [Mg^{2+}], the high-crosslinking 'kinase-on' state of the sensor will be dominant, and the corresponding activity of the autokinase will be dictated by α*K_{AK}. The midpoint of transition will depend on the relative magnitudes of all the parameters. However, the range of behaviors possible by this model of coupling depends heavily on the intrinsic equilibria of the sensor and autokinase themselves (K_{Sen}, K_{AK}). We observed that the two-domain model in **Figure 5B** captures much of the phenotypic behavior of the mutants shown in **Figure 2C**. However, different effects were observed for decoupling before and after the HAMP domain (**Figure 3, 4**) indicating that it needs to be treated as a separate domain with its own equilibrium constant and independent coupling to both the sensor and catalytic domains.

Three-domain allosteric coupling mechanism of signal transduction

Based on the results of Gly_7 insertion mutants and our inability to fully explain our data set with two-domain model, we developed a three-domain model, with allosteric couplings defined before and after the HAMP domain. In this model, the HAMP domain has its own intrinsic equilibrium, K_{HAMP}, and there are two coupling constants that describe how the sensor couples to the HAMP domain (α_1), and how the autokinase couples to the HAMP domain (α_2). All possible state transitions are enumerated in **Figure 6A**. This treatment allows for semi-independent modulation of the sensor and autokinase using the intrinsic equilibrium of the HAMP domain in the following ways. In the case where $\alpha_2 = 1$, the autokinase is decoupled from the sensor + HAMP. In this scenario, the HAMP domain can modulate the $[Mg^{2+}]$ dependent state transition of the sensor through coupling via α_1 without altering the basal autokinase activity, as shown in **Figure 6B**. In the case where $\alpha_1 = 1$, the sensor is decoupled from the HAMP+autokinase, and the HAMP domain can modulate the basal (and ligand-insensitive) activity of the autokinase through coupling via α_2, as shown in **Figure 6B**. When the protein is fully coupled (i.e. $\alpha_1, \alpha_2 \neq 1$), we can potentiate the 'kinase-on' or 'kinase-off' states of the sensor and autokinase in a manner that depends on both K_{HAMP} and α_n's, as shown in **Figure 6C**. Of particular interest is the case where $\alpha_1, \alpha_2 < 1$, which enables the simultaneous potentiation of the 'kinase-off' state, while maintaining the correlated sensor-autokinase behavior of PhoQ. This matches our observation that the 'kinase-off' states of both the sensor and autokinase were potentiated by the HAMP domain in our Gly_7 insertion experiments (**Figure 3**). Other possible behaviors with this 3-domain model include correlated sensing with 'kinase-on' potentiation, and anticorrelated signaling.

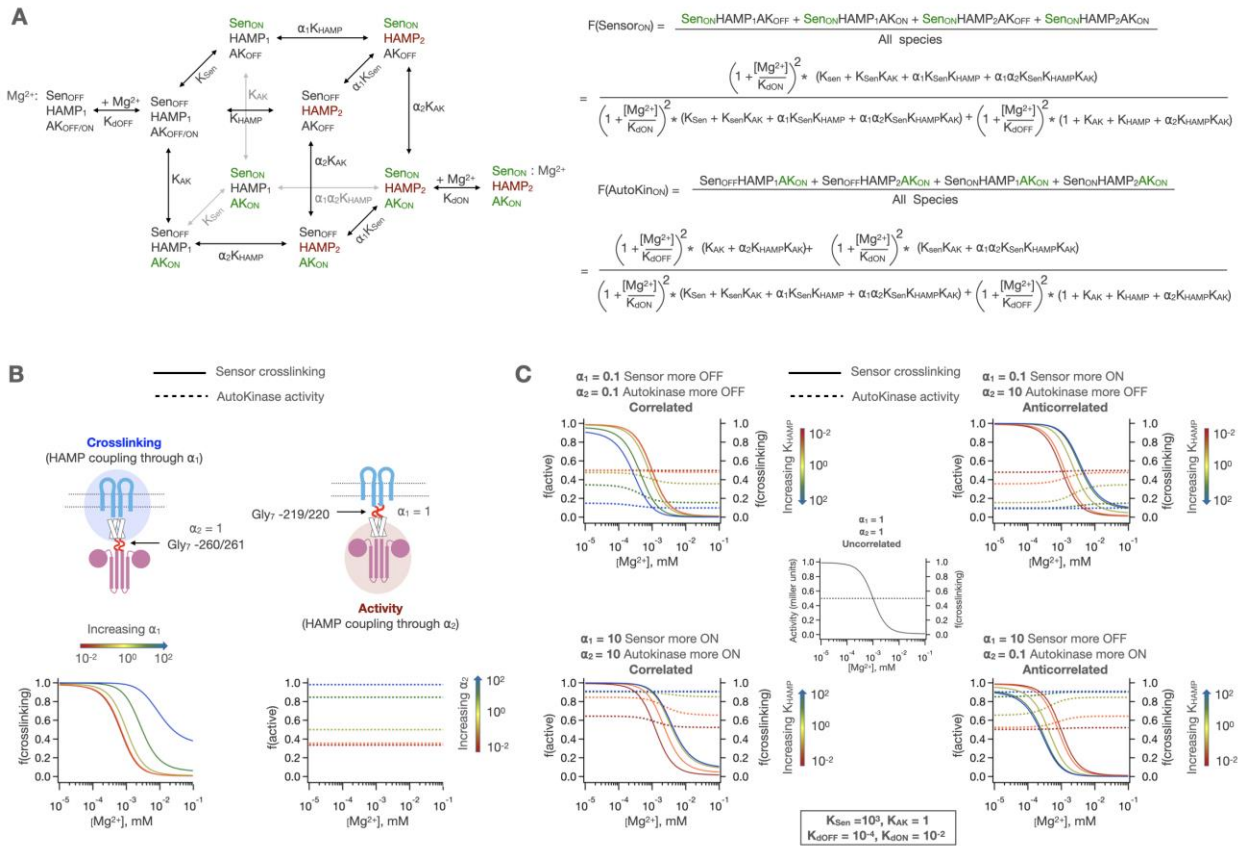

Figure 6 - 3-domain allosteric coupling model for PhoQ signaling. A) The HAMP domain is allowed to sample a two-state equilibrium between '$HAMP_1$' and '$HAMP_2$' states with the equilibrium constant K_{HAMP}. The sensor and autokinase domains of PhoQ are allowed to sample both 'kinase-on' and 'kinase-off' signaling states while coupled to '$HAMP_1$' state in adjacent HAMP domain with equilibria K_{Sen} and K_{AK} respectively. When adjacent states are in 'kinase-on' or '$HAMP_2$' states, the equilibria for transition are scaled by α_1 (sensor-HAMP) or α_2 (HAMP-autokinase). Predicted fraction of sensor crosslinking or autokinase activity are computed as shown to the right. Please note that Mg^{2+} binding is allowed for all eight possible signaling states but are omitted except for two reference states for clarity. Similarly, three equilibria arrows and constants have been shaded grey to spatially differentiate them from nearby equilibria. **B)** The HAMP domain allows for the independent modulation of the basal state of the sensor or autokinase. When $\alpha_2 = 1$, the HAMP domain modulates the $[Mg^{2+}]$ dependent transition of the sensor, and when $\alpha_1 = 1$, the HAMP domain modulates the basal activity level of the autokinase. **C)** the two allosteric coupling constants allow for both correlated and anticorrelated modulation of sensor and autokinase and allow for potentiation of both the 'kinase-on' and 'kinase-off' states.

In order to fit our semi-empirical models to experimental observations, we generated a set of 35 single-point mutants and Gly_7 insertions and *simultaneously* determined the sensor-crosslinking and autokinase activity at 5 different concentrations of Mg^{2+}. In addition to point-mutations along the signal transduction pathway, we inserted Gly_7 sequences between TM and HAMP domains (Gly_7 219/220), as well as between the HAMP and autokinase in two locations

(Gly$_7$ 260/261, Gly$_7$ 270/271) to disrupt interdomain coupling. We chose to insert Gly$_7$ both before and after the S-Helix motif (res 261-270) since this entire region is considered a coupling motif between the HAMP and Autokinase. We also included Gly$_4$ insertion at 260/261 which suffices as an alternate insertion for decoupling HAMP from autokinase. Finally, we combined Gly$_7$ insertions with some point mutations that show behavior markedly different from WT (S217W, E232A, N255A, Y265A) to further differentiate between changes in domain two-state equilibria and changes in interdomain allosteric coupling.

Using this set of mutants, we next determined the five core allosteric parameters (K_{Sen}, K_{HAMP}, K_{AK}, α_1, α_2), and the dissociation constants for Mg^{2+} to the two sensor states (K_{dOFF}, K_{dON}, **Figure 6A, Figure 7A**). One last parameter (S) is a scaling factor that relates the mole fraction of autokinase in the 'kinase-on' state to the experimentally observed Miller units associated with the beta-galactosidase transcription, which were obtained under strictly controlled experimental conditions to assure uniformity between mutants. In all, we sought to determine eight constants for each mutant. However, given the spacing of the points in our dose-response curves, it is only possible to obtain three pieces of information, i.e., the top, bottom and midpoint of the curves. Thus, with only six pieces of information (3 each from crosslinking and transcriptional activation) for each mutant, the model is under-determined for any one mutant. We avoid this problem by using global fitting. For a given mutant, only one or two (or in a single occasion, three) of the parameters are allowed to vary, with the others being fit as global parameters that are shared with other mutants. The choice of which parameters to vary is determined by the location of the perturbation on the primary sequence of PhoQ (**Figure 7-figure supplement 1**, see methods). For example, a mutation near the N-terminus of the HAMP domain would be expected to primarily alter α_1 and K_{HAMP}, so these values were allowed to vary

locally. Mutations near the center of the tertiary structure of the HAMP domain are allowed to vary K_{HAMP} alone and so on. This results in an overall fit with 62 adjustable parameters corresponding to 8 global parameters, 47 locally varied parameters, and 7 parameters fixed to a value of 1 to account for Gly_7 insertions (**Table 1**). By comparison, there are 6 * 36 = 216 observables. Thus, in theory, the data should be more than sufficient to define the independent parameters.

This model was globally fit using our mutant dataset as explained in detail in the Methods section. Briefly, we standardize the ranges of autokinase activity measurements (Miller units from beta-galactosidase assay) by the global average activity in our dataset. This normalizes the range of autokinase activity to one that is similar to crosslinking fractions (range 0 to 1) and gives both types of experimental measurements similar weights in our global fits. We give additional weight to data with experimental replicates (and hence greater certainty) by simply treating each replicate as an independent data set, with all the variables held constant between replicates during fit. Each parameter is allowed to sample a 10-log range of possible values, and the best fit is determined by minimizing the sum of residuals across the entire dataset. In order to avoid getting trapped in any local minima of the parameter space, we repeat the fit 125,000 times using randomly generated starting values for each parameter and determine confidence intervals for our parameters using bootstrapping to generate over 3000 synthetic dataset fits (see Methods for details). Where mutations or insertions have been introduced, we allow the parameters expected to be affected by the mutation to vary locally for the corresponding data set. Moreover, six mutants can be fit with fewer local parameters than were utilized in the fit, as the values for some of these locally fit parameters remain close to the globally fit value (within 10%), as highlighted in **Table 1** (green).

We are able to obtain a remarkably good fit for our entire dataset with the aforementioned considerations. **Figure 7** shows the results of the best obtained fit for 'wild type' PhoQ (Y60C) sensor-crosslinking (**Figure 7B**) and autokinase activity (**Figure 7C**). Since the WT data were fit entirely globally, they represented the most stringent test for the performance of our model overall, and qualitatively showed good agreement between model fit and experimental data. The values of the eight global parameters corresponding to this wild type fit are shown in **Figure 7D**, alongside two metrics of fit quality. The first metric is a bootstrapped confidence interval, with the frequency histogram of resulting fit values shown in the top panels. The second metric is a parameter sweep analysis in which the global sum of residuals is evaluated as the value of the indicated parameter is allowed to vary while all other parameters are held fixed. Five of our global parameters, K_{dOFF}, K_{dON}, K_{Sen}, K_{HAMP} and α_1 show excellent convergence to the 'best fit' value, with well-defined minima in the sum of residuals as we explore parameter value. Three parameters, K_{AK}, S and α_2 show strong signs of covariability, and wider confidence intervals. In the fully activated state, the observed signal is defined by the product of the scaling factor, S, and the fraction of the protein in the 'kinase-on' state (approximately $S*K_{AK}$). This product is well-defined and converges to a value of ≈ 1.02. However, as K_{AK} is lowered below this value, S increases in parallel to maintain a constant value for the product of $S*K_{AK}$. In **Figure 7-figure supplement 2**, we show that when the values of S are restrained, the values of K_{AK} are also restrained, and vice versa. Nevertheless, we can place a functionally meaningful upper limit on K_{AK}, of approximately 0.1. Similarly, we can place an upper limit on the value of 0.1 for α_2, which represents the negatively cooperative coupling of K_{AK} to the parameters defining the other domains. α_2 describes the difficulty of the autokinase to transition into the 'on-state' when coupled to the $HAMP_2$ state vs the $HAMP_1$ signaling state. Our data show that this transition is

disfavored. **Figure 7-figure supplement 3** shows that for both peaks of α_2 values centered around 10^{-2} and 10^{-7}, we converge to similar parameter fits for the other global parameters since both values of α_2 establish a tightly coupled 'kinase-off' state within the sensitivity of our experiments. Therefore, these uncertainties do not affect any of our conclusions below, which depend on presence of strong versus weak and negative versus positive coupling. We also examined the ability to fit a simpler two-domain allosteric coupling model (**Figure 5B**, see Methods Equation 2) to our data. This model failed to globally fit the set of sensor crosslinking and kinase activities of WT PhoQ, point mutants and Gly_7 insertions (**Figure 7-figure supplement 4**).

One feature that was somewhat surprising was that K_{AK} was unfavorable towards forming the 'kinase-on' versus 'kinase-off' states ($K_{AK} < 1$), even at limiting low concentrations of Mg^{2+}. This indicates that the observed activity for the WT protein is less than what is observed for some of the mutants, and what might be observed in a hypothetical state in which the autokinase is unfettered by connections to HAMP and the membrane. Although unexpected, this finding is consistent with a large body of data (65–67), and has been observed in PhoQ with antimicrobial peptide stimulation (68). Thus, in ligand-responsive HKs, evolution does not drive towards maximal activity which might lead to wasteful and toxic transcription, but instead a finely tuned value that is titrated to the degree of transcription required for function.

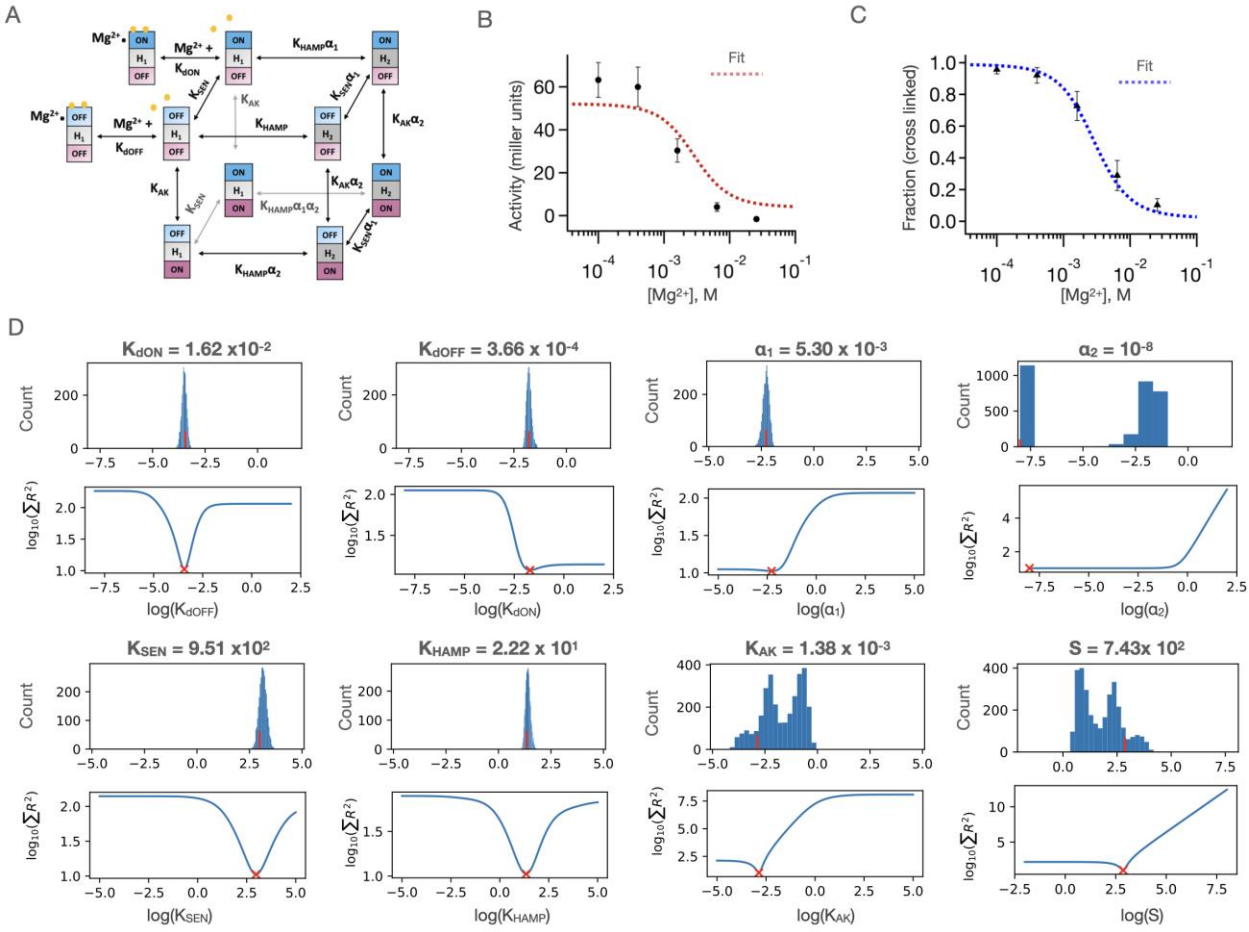

Figure 7 – Results of three-domain two-state allosteric model fit of PhoQ activity. **A)** Three-domain two-state allosteric model used for fitting (see also **Figure 6A**) **B)** Fits to the [Mg^{2+}]-dependent kinase activity and **C)** sensor crosslinking for 'wild type' Y60C PhoQ are shown. Error bars correspond to ± SD for n=9 biological replicates. **D)** Bootstrapped confidence intervals (top) and residual sweep analyses (bottom) are shown for all 8 global parameters. The value of the fit is indicated with red (x) and (|) marks. The confidence intervals of parameters S, K_{AK} and α_2 are further parsed in **Figure 7-figure supplement 2**, and the confidence intervals for α_2 are further parsed in **Figure 7-figure supplement 3**.

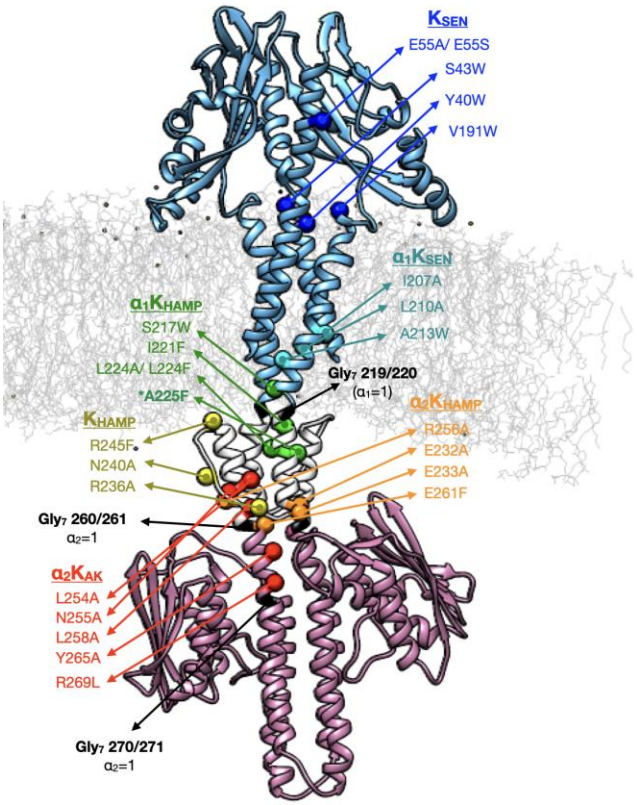

Alter membrane/interfacial interactions:
Y40W, S43W, V191W, A213W, S217W

Alter steric packing:
I207A, L210A, I221F, L224A, L224F, A225F, L254A, L258A, Y265A

Intradomain hydrogen bonding/stabilizing interaction:
E55A, E55S, N240A, R254F

Hypothesized tertiary contacts:
E232A, E233A, R236A, R256A

Conservation in HKs:
N255A, E261F, R269L

Uncouple domains:
Gly_7 219/220, Gly_4 260/261, Gly_7 260/261, Gly_7 270/271

Constraining parameter space:
S217W + Gly_7 219/220, S217W + Gly_7 260.261, E232A + Gly_7 260/261, N255A + Gly_7 260/261, Y265A + Gly_7 219/220, Y265A + Gly_7 260/261

Figure 7-figure supplement 1 – Point mutations and Gly7 insertions in PhoQ. A molecular dynamics model of PhoQ shows the location of mutations on 1 monomer with colored Cβ spheres. Colors correspond to mutation labels in **Figure 8**.

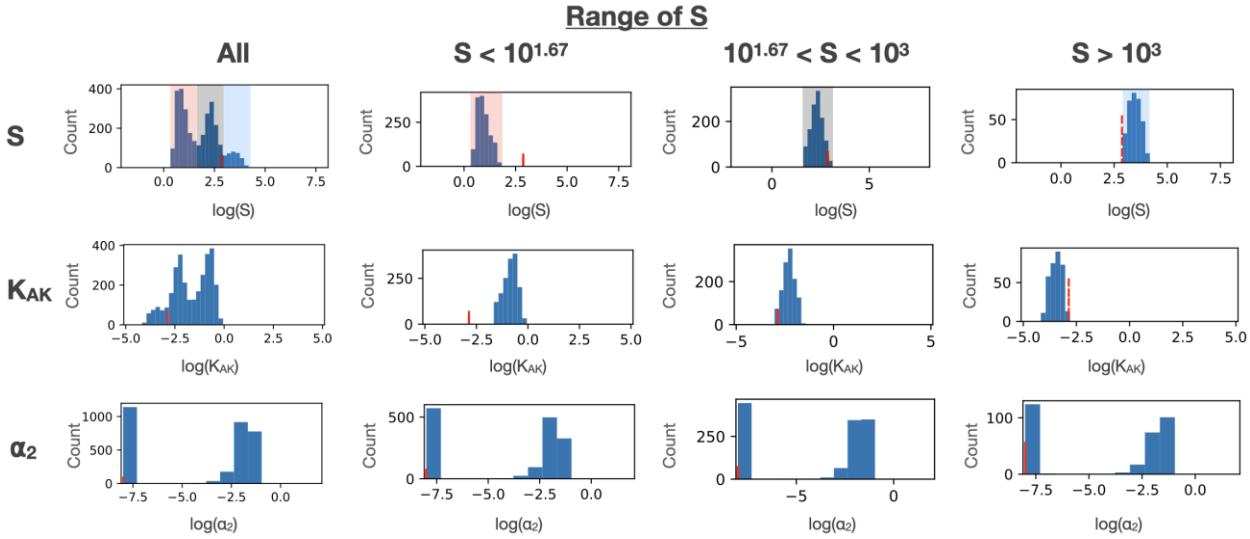

Figure 7-figure supplement 2 – Effect of constraining S and K_{AK}. The confidence intervals for K_{AK} and α_2 parameters are shown as a function of different ranges of S values. S and K_{AK} show strong correlation.

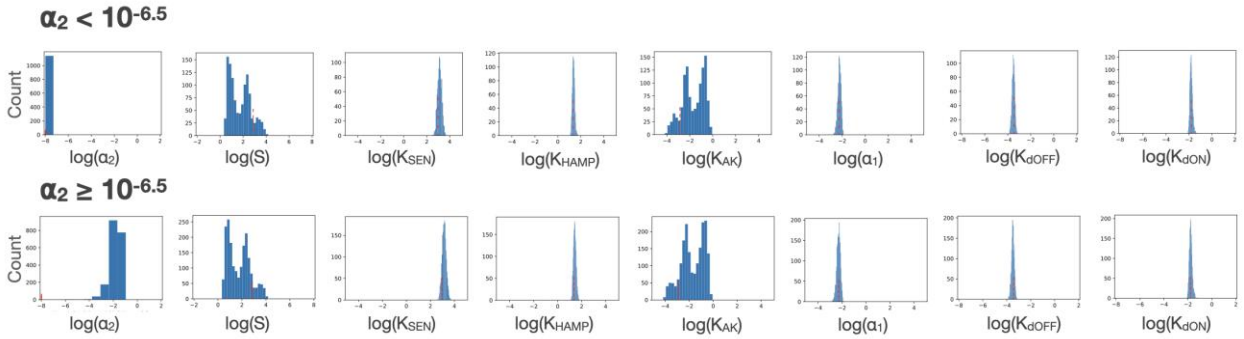

Figure 7-figure supplement 3 – Effect of constraining α_2. The confidence intervals for all global parameters are shown as a function of different ranges of α_2 values.

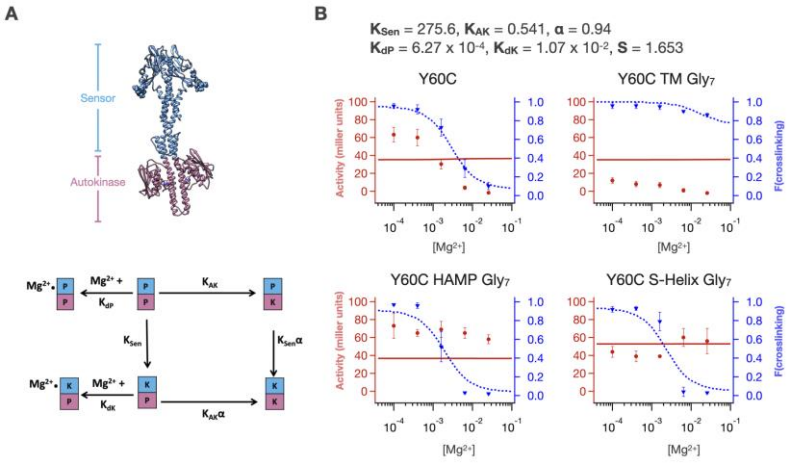

Figure 7-figure supplement 4 – A two-domain two-state allosteric coupling model does not fit set of PhoQ mutants. A) In a two-domain signaling model, PhoQ is split into two domains, the 'Sensor' which includes the periplasmic PAS domain, TM and HAMP domains, and the 'Autokinase'. These two domains have their own intrinsic equilibria, K_{Sen} and K_{AK}, which are coupled in their 'on' states by the parameter α. The population ensemble is perturbed by Mg^{2+} binding to both states of the Sensor. **B)** Global fitting of PhoQ single point mutant and Gly_7 insertion data set cannot simultaneously fit sensor crosslinking and autokinase activity data. Representative fits for WT phoQ and Gly_7 disconnections are shown.

Application of the 3-domain model to a set of mutants illustrates how substitutions distant from active sites modulate signal strength and ligand sensitivity.

The values of the parameters provide a detailed view of the energy landscape of PhoQ, in the 'kinase-on' and 'kinase-off' state – and how it is modulated by binding to Mg^{2+} and mutations. The parameters are consistent with our observations that the HAMP domain is a significant modulator of the intrinsic equilibria of the sensor and autokinase domains. At high Mg^{2+} concentrations, PhoQ is in a 'sensor-off' and 'autokinase-off' state. With respect to this

reference ‘kinase-off’ state, the HAMP domain has a thermodynamically favored signaling state, ‘$HAMP_2$’, with a fit equilibrium value of $K_{HAMP} = 22$. This favored state of the HAMP domain is more strongly coupled to these ‘kinase-off’ states and serves to dampen the otherwise favorable transitions of both the sensor and autokinase domains to the ‘kinase-on’ conformation. The sensor’s propensity to switch to a ‘sensor-on’ state is reduced from a highly preferred equilibrium $K_{Sen} = 9.5 \times 10^2$, to a modest downhill equilibrium of $\alpha_{1*}K_{Sen} = 5.0$ when the HAMP domain is in this $HAMP_2$ state. This latter equilibrium is weak enough to be overcome by Mg^{2+} binding, and the ‘sensor-off’ state is further stabilized with more ligand binding. The ‘$HAMP_2$’ state that is preferred in this ‘sensor-off’ state is also strongly coupled to the ‘kinase-off’ state of the autokinase, reducing the propensity of the autokinase to switch to the ‘kinase-on’ state from $S{*}K_{AK} = 1.0$ to $\alpha_{2*}S{*}K_{AK} \leq 10^{-3}$. Thus, the $HAMP_2$ state behaves as a negative modulator of the intrinsic propensities of the sensor and autokinase. At high enough [Mg^{2+}], the entire population ensemble is predominantly in the $sensor_{OFF}$-$HAMP_2$-$Autokinase_{OFF}$ state.

In the absence of ligand, the sensor’s modest downhill equilibrium to the ‘kinase-on’ state is strongly tied to a switch of the HAMP domain from ‘$HAMP_2$’ to ‘$HAMP_1$’, with an equilibrium = $1/(\alpha_1 K_{HAMP}) = 25$. The $HAMP_1$ state is weakly coupled to the autokinase, which allows the autokinase to sample both kinase-off and kinase-on state, with an effective equilibrium of $S.K_{AK} = 1.02$. This allows for the partial decoupling of the sensor and the autokinase at low Mg^{2+} concentrations observed in wild type PhoQ (**Figure 2C**) with the population ensemble composed of both $sensor_{ON}$-$HAMP_1$-$Autokinase_{ON}$ and $sensor_{ON}$-$HAMP_1$-$Autokianse_{OFF}$ states. Because the $HAMP_1$ state is weakly coupled to both adjacent domains, the equilibria constants K_{Sen} and K_{AK} are close to the intrinsic equilibria of these domains when uncoupled from the HAMP domain altogether. In other words, $K_{Sen} = 9.5 \times 10^2$ reflects the high

propensity of the sensor to switch to the 'sensor-on' state when uncoupled from the HAMP domain, and $S.K_{AK} = 1.0$ reflects the propensity of the autokinase to have as high an activity as WT PhoQ at low [Mg^{2+}], as shown earlier with Gly_7 disconnections in **Figure 3**.

The parameters for individual mutations show how amino acid substitutions alter the energy landscape and how these changes in turn alter the phenotype. Before discussing the effects of substitutions, however, it is important to address the overall quality of the fit over the full ensemble of mutants. **Figure 8** shows the results of fits for our mutations and Gly_7 insertions with mutations color-labeled according to the locally varied parameters as in **Figure 7-figure supplement 1**. The corresponding fit values are listed in **Table 1**, and confidence intervals and parameter sensitivity analyses are shown in **Figure 8-figure supplement 1**. While it is possible to construct models with even more states, e.g., by treating the TM domain separately rather than as an extension of the sensor domain, the number of parameters – and their uncertainty- rapidly increases. We therefore chose the simplest model required to describe the entire set of data.

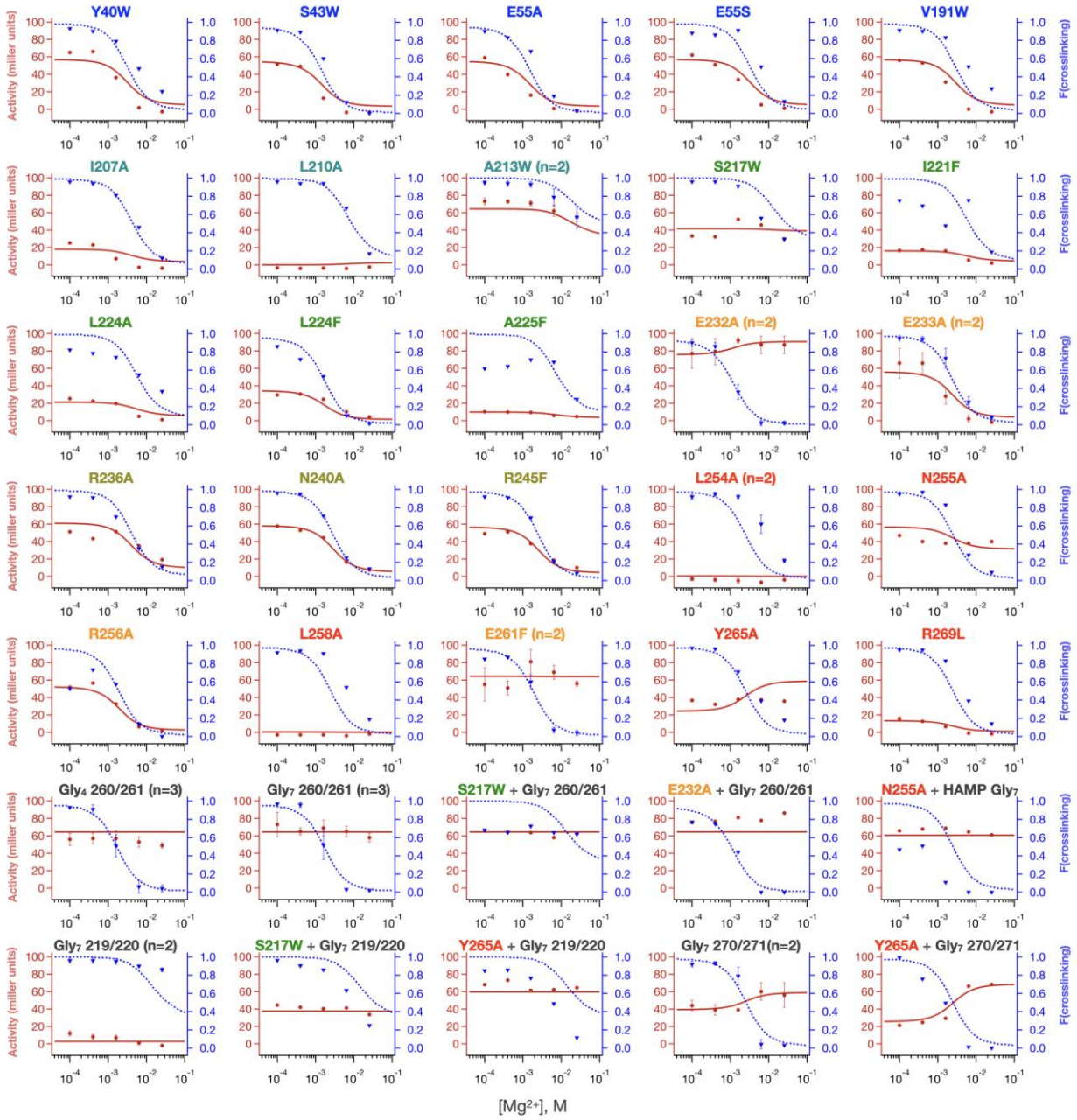

Figure 8 – Local fits of sensor crosslinking and kinase activity for 35 PhoQ mutations. Fits to activity (red line, closed circles) and sensor crosslinking (blue dashed line, triangles) are shown for the entire PhoQ dataset. The color of mutations matches the color scheme in **Figure 7A** to indicate locally varied parameters, and these parameters are listed in **Tables 1** and **2**. Confidence intervals and residual sweep analyses are presented in **Figure 8-figure supplement 1**. Poor fits are highlighted in **Figure 8-figure supplement 2**.

Figure 8-figure supplement 1 – Bootstrapped confidence intervals and residual sweep analyses for PhoQ mutant fits. Histograms from 3061 convergent fits of simulated datasets for each local variable are shown in top panels. Residual sweeps in which the sum of residuals of the global fit is plotted as a function of indicated parameter being varied locally is shown in the bottom panels. Values of parameter fits are shown with red (x) and (|) marks.

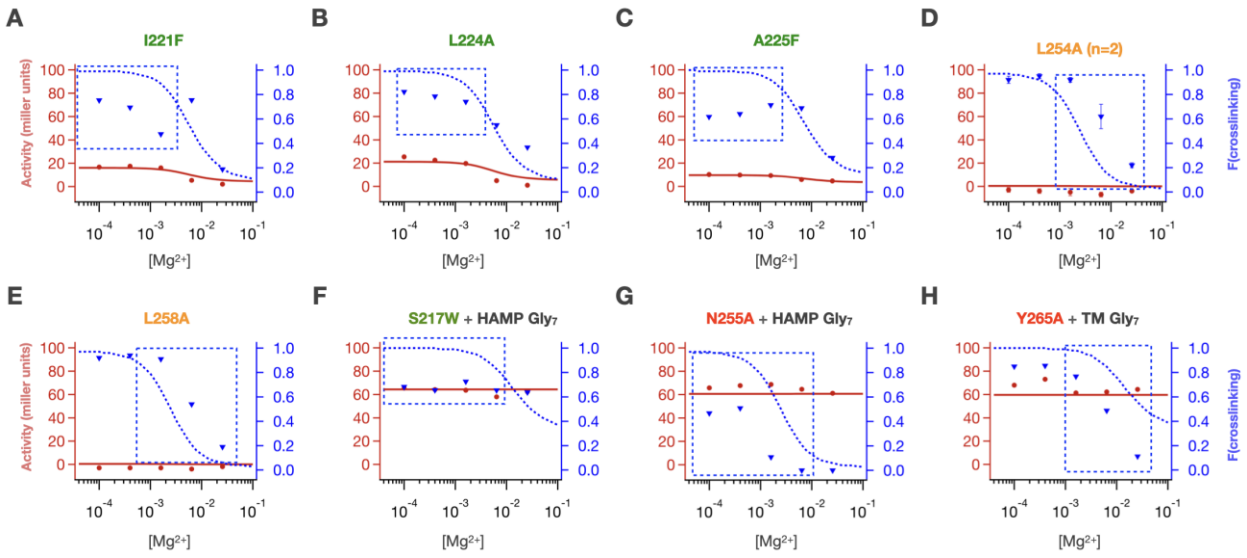

Figure 8-figure supplement 2. Poor fits were obtained for crosslinking at low [Mg^{2+}] for **(A)** I221F, **(B)** L224A and **(C)** A225F. Poor midpoints of crosslinking transitions were fit for **(D)** L254A and **(E)** L258A. Some combinations of mutations had poor crosslinking fits **(F)** S217W + HAMP Gly_7, **(G)** N255A + HAMP Gly_7 and activity fits **(H)** Y265A + sensor Gly_7

We obtained fits within experimental error for the [Mg^{2+}]-dependent transcriptional activity of our entire mutant data set. Thus, the model worked well for all ligand-sensitive mutants. The only deviations lay in the crosslinking data for non-functional mutants that were decoupled in the transcriptional output (**Figure 8-figure supplement 2**). One such set of mutants (I221F, L224A and A225F) had substitutions at the C-terminal end of the second TM helix. While the midpoint and lower limit were well described by the model, the experimentally observed extent of crosslinking reached an upper limit of 65% to 80% crosslinking at low Mg^{2+}, less than the predicted value near 100%. Given the location of the substitutions near the membrane interface, it is possible that a portion of the protein is not fully inserted and hence the samples used for western analysis might have been contaminated by cytoplasmically localized, and not yet membrane-inserted protein, which would be expected to remain not cross-linked. There are also two mutations localized near the interface between the HAMP and the autokinase domains where the mid-point is poorly fit (L254A, L258A), potentially owing to our choices of parameters to locally float for these mutants (**Figure 8-figure supplement 2D-E**) as discussed in

584 Methods. Significantly better fits were obtained by altering the parameters varied for these
585 mutants from K_{HAMP} and α_2 to K_{AK} and α_2. Thus, these residues may be involved in the
586 underlying equilibrium of the autokinase domain itself due to their proximity to the "S-helix"
587 that connects the HAMP domain to the autokinase. Finally, double mutants are not fit well,
588 especially when the two sites of mutation are in close proximity (S217W + HAMP Gly_7, N255A
589 + HAMP Gly_7, Y265A + Sensor Gly_7, **Figure 8-figure supplement 2F-H**). This is likely
590 because the thermodynamic effects of double mutations are often non-additive in structurally and
591 sequentially proximal positions that interact directly. Additionally, while we observe relatively
592 invariant expression of almost all variants (as seen in the western analysis used to quantify
593 crosslinking), some variants, particularly double mutants required slight induction of expression
594 with 10 μM IPTG for observable levels of membrane-inserted PhoQ by western-blotting (see
595 Methods). In summary, the crosslinking and transcriptional activity data are very well fit for the
596 entire set of mutants, except for a fraction of the nonfunctional mutants in which Mg^{2+} binding
597 and transcription were significantly decoupled. Even for these mutants, however, there is a
598 qualitative fit to the data, and possible reasons for the deviation.
599 Our results illustrate how allosteric coupling of domain equilibria changes in response to
600 single-site substitutions. Although we chose a collection of mutations that were not involved in
601 Mg^{2+} binding and catalysis, we observed a large range of effects on the transcriptional response
602 of the mutants, including an inverse response in E232A and Gly_7 270/271 insertion. The
603 advantage of the current analysis is describing how these mutations alter the energetics of
604 individual domains, and their coupling to adjacent domains. As an organism evolves to match its
605 environment, its sensory systems need to adjust to the ligand-sensitivity (midpoint of the dose-
606 response curve), the magnitude of the increase in the response (in this case, the activity in the

607 absence of Mg^{2+}/activity in presence of Mg^{2+}) and the basal activity (in the presence of saturating
608 Mg^{2+}). We consider these features separately.

609 In a well-coupled system such as WT PhoQ, the midpoint can be modulated by point
610 mutations anywhere along the signal transduction pathway between the sensor and the
611 autokinase. The only requirement is for the substitution to have an effect on the internal
612 equilibrium constant for the kinase-promoting versus the phosphatase-promoting conformations
613 of the domain that houses the mutation. So long as the domains are tightly coupled, then an n-
614 fold change in the internal equilibrium will translate to an n-fold change in the midpoint of the
615 overall dose-response curve. Moreover, as the couplings α_1 and α_2 become less strong, the
616 magnitude of the shift in the dose response curve is decreased. Thus, it is not necessary to change
617 the binding interactions with the metal ions to affect changes in the ligand sensitivity of the
618 system which provides the system a wealth of opportunities to tune sensitivity.

619 The fractional change in the kinase activity that can be achieved upon saturation of the
620 ligand-binding sites is a second factor, which ranges with the requirements of a system. For
621 example, the change in transcriptional response in PhoQ is modest, reaching about a factor of 5
622 to 20-fold change, while other two-component systems such as VirA have a dynamic range as
623 large as 10^5 (66, 69–71). It is however possible that combinatorial signals might further increase
624 the overall kinase activity of PhoQ from that observed at low Mg^{2+}, owing to additive
625 modulation of the sensor domain by other stimuli (H^+, antimicrobial peptides, MgrB, SafA,
626 UgtL (72)), as some independence between signal inputs has been demonstrated for *S.*
627 *Typhimurium* PhoQ (73). For simple systems that respond to a single ligand, the maximal
628 response is defined by the ratio of the intrinsic affinities of the ligand for the ‘kinase-on’ versus
629 ‘kinase-off’ conformations (K_{dON}/K_{dOFF}). Mutations that decrease the coupling attenuate the

maximal response, and the system becomes decoupled when α_1 or α_2 reaches 1. The maximal response in absolute terms is another factor, which depends on the kinetic efficiency of the underlying autokinase domains. When untethered from the remainder of the protein, the autokinase domain shows large increases activity (**Figure 3**), so the role of the remainder of the protein can be seen as a negative regulation. Indeed, we find that K_{AK} is significantly less than 1, and this value can be positively modulated by some mutations that reach transcriptional levels somewhat greater than WT for PhoQ. In summary, there is a diversity of mechanisms that nature can call upon to alter the activity of HKs, as illustrated in a relatively small sampling of the 35 mutants studied here.

Discussion

It has been appreciated for several decades that the effector domains of multi-domain signaling proteins can produce responses that are either potentiated or diminished relative to the change in state of sensory domains that drive these responses. S J Edelstein and J P Changeux in seminal work coined the terms “hyper-responsive” and “hypo-responsive” to define this uncoupled behavior between domains (74), which has since been examined in other classes of multi-domain signaling proteins such as GPCRs (75–77). In this work, we examine the coupling behavior between the sensor and effector domains of transmembrane bacterial sensor histidine kinases and possible roles of modularly inserted signal transduction domains in optimizing this coupling behavior using a model gram negative HK, PhoQ. We find that the intervening HAMP signal transduction domain is necessary to assemble an overall bistable histidine kinase from Mg^{2+}-sensor and autokinase-effector domains that are too biased to one signaling state (‘kinase on’ state). This is accomplished by strongly coupling the thermodynamically preferred state of the HAMP domain to the disfavored ‘kinase off’ signaling states of sensor and autokinase,

opposing these otherwise strong equilibria such that the overall assembly is bistable and significantly modulated by ligand binding (**Figure 9**). Thus, the HAMP domain does more than transmit the response; it instead serves to tune the ligand-sensitivity amplitude (i.e. minimum and maximum signal and midpoint of transition) of the response.

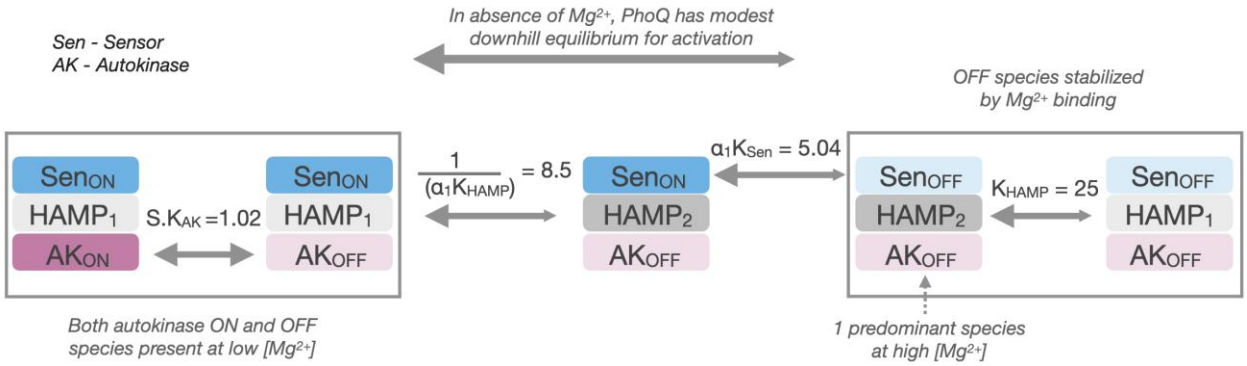

Figure 9 – Allosteric pathway for PhoQ activation. In the absence of Mg^{2+}, PhoQ has a moderate downhill equilibrium to a mixture of active states. Mg^{2+} binding is sufficient for overpowering this equilibrium and stabilizing the 'kinase-off' state, resulting in a predominantly Sensor-off/HAMP2/Autokinase-off population.

Evolutionarily, the insertion of signal transduction domains in HKs could allow for the facile modulation of the intrinsic equilibria of sensor and effector domains and their coupling behavior, which may be more difficult to alter through the direct mutation of these domains themselves. The sequence and subsequent structures of sensors and autokinase domains are subject to many evolutionary constraints, be it the specificity and affinity for ligands in sensor domains, the specificity for membrane homodimerization of HKs (78), or the cognate specificity for response regulator (13, 79–82) and the ability to inhabit and switch between the various conformations required for a full catalytic cycle in the autokinase domain (15). Furthermore, most two-component systems feature multiple accessory protein components involved in sensing, feedback regulation and cross-talk with other signaling systems, which add evolutionary constraints to these domains (83). In the closely related class of chemotaxis proteins, the analogous transmembrane protein is also subject to extensive covalent modifications that modulate activity. When all these evolutionary activity and specificity considerations are met,

675 the resulting domain may not be ideally bi-stable in isolation. Indeed, in PhoQ, we find that both
676 sensor and autokinase highly prefer the 'kinase-on' state, and therefore cannot be allosterically
677 connected to make an overall bistable protein capable of being converted to the 'kinase-off' state
678 by Mg^{2+} binding. The presence of one or more signal transduction domains allows for two
679 advantageous considerations for producing and fine-tuning overall HK bistability; the
680 thermodynamic stability of the signal transduction domain can be used to preferentially stabilize
681 or destabilize a given signaling state of sensors or autokinases indirectly through allosteric
682 coupling, and the strength and even direction of coupling can be easily modulated through
683 mutations at the domain junction, rather than mutations that may alter the core functions of the
684 sensor/autokinase themselves. In the case of PhoQ, the HAMP is an allosteric repressor of
685 autokinase activity; as such, mutations that destabilize the thermodynamically preferred HAMP
686 state ($HAMP_2$) or reduce its coupling to the autokinase would allosterically increase kinase
687 activity and vice versa.

688 The latter phenomenon is especially potent in the context of alpha-helical coiled-coil
689 connections between domains of HKs, in which a drastic change in coupling or thermodynamic
690 stability can be caused by minor sequence insertions, deletions and alterations due to the highly
691 regular and cooperative nature of coiled-coil stabilizing interfaces. We have shown that the
692 insertion of a stretch of glycine residues is sufficient to almost completely uncouple domains. On
693 the other extreme, a well folded coiled coil junction can create strong allosteric coupling due to
694 the cooperative folding and stability of such a motif. A range of stabilities can be achieved by
695 various means, including the insertion or deletion of one or more residues to disrupt the
696 canonical heptad pattern of hydrophobic residues of the dimeric core of the protein, as is often
697 observed in the conserved S-helix motif, which connects HAMP to autokinase domains in HKs

(84). Schmidt *et. al.* (85) showed that crystal structures of cytoplasmic domains in different conformations accommodate the structural deviations of these S-Helix sequence insertions by delocalizing the strain over different lengths of the proximal alpha-helical core. These different "accommodation lengths" could be analogous to the different strengths of allosteric coupling depending on the signaling states of the adjacent domains in our equilibrium signaling model. We also find conservation of glycine motifs and helix-disrupting proline residues in the juxta-membrane regions of chemotaxis proteins and HKs respectively (65, 86, 87), which hint at the significant modulation of allosteric coupling strength by the alteration of helical and coiled-coil geometries. In some systems, domains are even segregated to entirely different proteins, in which case the strength of the protein-protein interaction between components can be altered to vary allosteric coupling. These are all evolutionarily accessible solutions to fine-tune the function of a histidine kinase.

Finally, this evolutionary argument may also explain the lack of a parsimonious structural mechanism for signal transduction, even in HKs with a specific domain architecture. Although this problem is exacerbated by the dearth of multi-domain structures of HKs in various signaling conformation, several signaling hypotheses have been put forward regarding the structural mechanism for signal transduction in HKs, particularly in HAMP domains. These include the gear-box mechanism (AF1503, Aer2 multi-HAMP)(88), piston mechanism (Tar) (89, 90), scissoring mechanism (Tar, BT4663, PhoQ) (39, 91, 92), orthogonal displacement mechanism (HAMP tandems, Tar) (43, 93, 94) and the dynamic HAMP mechanism (Adenylate cyclase HAMP) (45, 95, 96). A recently elucidated set of structures of the sensor, TM and signal transduction domains of NarQ remains the only representative of a multidomain transmembrane structure of an HK containing a signal transduction domain, and again shows a rigid-body

bending transition of the HAMP domain about the conserved N-terminal proline between apo- and holo-states of the sensor (97).

It may be that signal transduction mechanisms in HKs are as varied as their modular architecture, and many structural transitions could account for the underlying function in signaling, which is the allosteric modulation of multi-state equilibria of adjacent domains in response to structural transitions caused by a sensory event. Indeed, the only requirement for signal transduction is a series of domains with two states that either favor or disfavor the kinase state, and a means to transmit the information between the states. Helical connections between domains provide efficient coupling, but the conformational changes within the domain need not be obligatorily the same for different domains. Additionally coupling can involve tertiary contacts, which can be used in conjunction with or instead of helical connections (11, 14, 15, 17, 98). Interestingly, the observation that PhoQ has a weakly HAMP-coupled 'kinase-on' state and a strongly HAMP-coupled 'kinase-off' state has been posited before, albeit in the context of a hypothesized tertiary contact between the membrane-distal portion of HAMP helix-1 and a loop in the autokinase domain (68). The idea that autokinase domains intrinsically have high-kinase activity and are subsequently inhibited by strong coupling to up-stream domains and the further stabilization of these inhibitory conformations by ligand-binding warrants examination as a generalizable signaling mechanism for histidine kinases.

Materials and Methods:

Materials:

BW25113 and HK knockout strains were obtained from the Keio collection. TIM206 (*E. coli* Δ*phoQ*, p*mgrB*::LacZ) was obtained from Tim Mayashiro (Goulian lab). pTrc99a (GenBank # M22744) was obtained from commercial sources. pSEVA311 (GenBank# JX560331) was

developed by the de Lorenzo lab and was a gift from the European Standard Vector Architecture consortium. Brilacidin was a gift from Polymedix Inc. N-ethylmaleimide (NEM) was purchased from Sigma. Tris-Acetate gels (Thermofisher Scientific) and Anti-PentaHis antibody (Thermofisher Scientific) were used for western blotting.

Methods:

Cloning: PhoQ mutants were cloned into the pTrc99a plasmid multiple cloning site by restriction cloning. Point mutations were made by quick-change mutagenesis and confirmed by sanger sequencing. Hybrid HK-gene reporter plasmids were built in pTrc99a plasmid by introducing a c-terminally 6x His-tagged HK construct into the IPTG inducible MCS, and the mCherry reporter sequence downstream by Gibson cloning (99). Sequences of reporters are available in supplementary methods. Gly_7 disconnections and point mutations were introduced by a blunt-end ligation strategy and confirmed by Sanger sequencing.

Growth of PhoQ constructs: For each biological replicate, an isolated colony of TIM206 (genotype: Δ*phoQ*, p*mgrB*::LacZ) containing various pTrc99a-*phoQ* constructs was grown overnight at 37 ℃ in MOPS minimal media + 50 µg/mL AMP and 1 mM $MgSO_4$. These overnight cultures were then diluted 50x into 1 mL MOPS media + 50 µg/mL AMP and 1 mM $MgSO_4$ and grown at 37°C for 2 hours. These cultures were further diluted 500X into 30 mL MOPS minimal media + 50 µg/mL AMP containing 0.1, 0.4, 1.6, 6.4 and 25.6 mM $MgSO_4$, and grown for at least 5 hours such that the density of the culture reaches log-phase (OD_{600} = 0.2 – 0.8). 500 µL of culture is removed for evaluating beta galactosidase activity, while the remaining culture is used for western analysis. Two constructs (A225F, Y265A Gly_7 260/261) showed no detectable PhoQ in membrane preparations and required induction with 10 µM IPTG during growth for observable levels of membrane-inserted PhoQ by western blot.

Beta galactosidase activity: 500 µL of PhoQ culture was combined with 500 µL of 1x Z-buffer + 40 mM beta-mercaptoethanol, 25 µL of 0.1% SDS in water, and 50 µL of chloroform in a glass culture tube and vortexed for complete lysis. The lysate was then prewarmed to 37°C in an air incubator before addition of ONPG substrate. 0.25 mL of prewarmed 4 mg/mL ONPG in 1x Z-buffer + bMe was added to the lysate to initiate hydrolysis, which was then quenched with the addition of 500 µL of 1M Na_2CO_3 after variable incubation periods. The quenched hydrolysis was then centrifuged to remove any cell debris, and absorbance at 420 nm and 550 nm was measured in triplicate using a Biotek synergy2 plate-reader with pathlength correction. Miller units were calculated as follows:

Miller units = $1000*(OD_{420} – 1.75*OD_{550})/(OD_{600}*\text{dilution factor}*\text{incubation time in min})$

Membrane fraction isolation: 30 mL of PhoQ culture was centrifuged at 4350xg at 4°C for 20 minutes to collect a cell-pellet. This cell pellet was immediately frozen in liquid nitrogen and stored at -80°C until analysis. Frozen pellets were thawed, suspended and incubated on ice with 500 µg/mL N-Ethylmaleimide (NEM) and 1 mg/mL lysozyme in 50 mM TRIS buffer, pH 8, for 1 hour. Cells were then lysed by 30 seconds of tip sonication (Fisher Scientific Sonic Dismembrator Model 500, 10% Amplitude, 1 sec pulse on, 1 sec pulse off). Lysed cells were then centrifuged at 16000xg for 10 minutes to remove cell debris. Membrane was isolated from the supernatant by further centrifugation at 90,000xg for 10 minutes. Membrane pellets were then resuspended in 1X lithium dodecyl sulfate (LDS, Invitrogen) loading buffer containing 8M urea and 500 mM NEM, boiled at 95°C for 10 minutes and analyzed by western blot.

Monomer and dimer quantification by western blot: LDS solubilized membrane prep samples were separated on 7% TRIS-SDS gels by electrophoresis at 200V for 70 min, and then transferred onto nitrocellulose membranes by dry transfer (iBlot2). Membranes were then

blocked using 1% BSA in TBS-t buffer (20 mM Tris, 2.5 mM EDTA, 150 mM NaCl, 0.1% Tween-20), probed using an anti-pentaHis HRP antibody, and visualized using luminescent ECL substrate on a BioRad imager. Bands corresponding to PhoQ monomer and dimer were quantified using Image-J software to yield a crosslinking efficiency between 0 and 1. A representative quantification of crosslinking is presented in **Figure 2 figure supplement 1**.

Measuring activity of CpxA, BaeS: HK constructs were cloned into the MCS of pTrc99a plasmid, and the associated fluorescent reporter gene was cloned downstream. For the CpxA reporter plasmid, the response regulator CpxR, was also cloned into the MCS and transformed into AFS51 strain (Δ*cpxA*Δ*pta*::Kan p*cpxP*::GFP) by heat shock transformation. For BaeS, the response regulator BaeR, was cloned into an additional plasmid, pSEVA331 under an IPTG inducible promoter and both plasmids were transformed into a Δ*baeS*Δ*cpxA* double KO strain by heat shock transformation. Cultures were started by diluting overnights 200-500 fold into fresh LB medium + 50 µg/mL AMP and allowed to grow to mid-log phase (OD_{600} = 0.4 – 0.6) before analysis by flow cytometry. The responsiveness of *cpxP* reporter was confirmed by treating log-phase cultures with 2 µg/mL brilacidin for 1.5 hours before analysis. Expression of HKs was confirmed by western analysis using the c-terminal 6x His-tag for quantification.

Flow cytometry: LB cultures at mid-log phase were diluted 20x into 1x PBS buffer and 20,000 cells gated by forward and side-scatter were evaluated for GFP fluorescence (p*cpxP*::GFP; Ex. 488 nm, Em. 515 nm) or mCherry fluorescence (p*spy*::mCherry, Ex. 488 nm, Em. 620 nm) per sample on a BD FACS caliber instrument. Sample average fluorescence and standard error were determined by standard analysis using Flo-Jo software.

Data Fitting: For data fitting, only data-sets in which kinase activity and sensor crosslinking have been determined simultaneously from the same samples at all 5 concentrations of Mg^{2+}

were included in analysis. The resulting kinase-active and sensor cross-linking-competent states are partitioned to generate expressions dependent on $[Mg^{2+}]$ as the lone variable as shown below. The parameters are then fit globally across all datasets, except for those accounting for the perturbation of a mutation/ Gly_7 disconnection, which are fit locally. Locally fit parameters are kept identical between replicates or additive mutations.

Equation 1: concerted model equation

$$F(ON) = \frac{PhoQ_{ON} + PhoQ_{ON}:Mg^{2+}}{PhoQ_{ON} + PhoQ_{ON}:Mg^{2+} + PhoQ_{OFF} + PhoQ_{OFF}:Mg^{2+}} = \frac{\left(1 + \frac{[Mg^{2+}]}{K_{dON}}\right)^2 * K}{\left(1 + \frac{[Mg^{2+}]}{K_{dON}}\right)^2 * K + \left(1 + \frac{[Mg^{2+}]}{K_{dOFF}}\right)^2}$$

Equation 2: two-domain two-state model fitting

$$F(Sensor_{ON}) = \frac{Sen_{ON}AK_{OFF} + Sen_{ON}AK_{ON}}{Sen_{ON}AK_{OFF} + Sen_{ON}AK_{ON} + Sen_{OFF}AK_{OFF} + Sen_{OFF}AK_{ON}} = \frac{\left(1 + \frac{[Mg^{2+}]}{K_{dON}}\right)^2 * (K_{Sen} + \alpha K_{Sen}K_{AK})}{\left(1 + \frac{[Mg^{2+}]}{K_{dON}}\right)^2 * (K_{Sen} + \alpha K_{Sen}K_{AK}) + \left(1 + \frac{[Mg^{2+}]}{K_{dOFF}}\right)^2 * (1 + K_{AK})}$$

$$F(AutoKin_{ON}) = \frac{Sen_{ON}AK_{ON} + Sen_{OFF}AK_{ON}}{Sen_{ON}AK_{OFF} + Sen_{ON}AK_{ON} + Sen_{OFF}AK_{OFF} + Sen_{OFF}AK_{ON}} = S* \frac{\left(1 + \frac{[Mg^{2+}]}{K_{dON}}\right)^2 * \alpha K_{Sen}K_{AK} + \left(1 + \frac{[Mg^{2+}]}{K_{dOFF}}\right)^2 * K_{AK}}{\left(1 + \frac{[Mg^{2+}]}{K_{dON}}\right)^2 * (K_{Sen} + \alpha K_{Sen}K_{AK}) + \left(1 + \frac{[Mg^{2+}]}{K_{dOFF}}\right)^2 * (1 + K_{AK})}$$

Equation 3: three-domain two-state model fitting

$$F(Sensor_{ON}) = \frac{Sen_{ON}HAMP_1AK_{OFF} + Sen_{ON}HAMP_1AK_{ON} + Sen_{ON}HAMP_2AK_{OFF} + Sen_{ON}HAMP_2AK_{ON}}{All}$$

$$= \frac{\left(1 + \frac{[Mg^{2+}]}{K_{dON}}\right)^2 * (K_{sen} + K_{Sen}K_{AK} + \alpha_1 K_{Sen}K_{HAMP} + \alpha_1\alpha_2 K_{Sen}K_{HAMP}K_{AK})}{\left(1 + \frac{[Mg^{2+}]}{K_{dON}}\right)^2 * (K_{Sen} + K_{sen}K_{AK} + \alpha_1 K_{Sen}K_{HAMP} + \alpha_1\alpha_2 K_{Sen}K_{HAMP}K_{AK}) + \left(1 + \frac{[Mg^{2+}]}{K_{dOFF}}\right)^2 * (1 + K_{AK} + K_{HAMP} + \alpha_2 K_{HAMP}K_{AK})}$$

$$F(AutoKin_{ON}) = \frac{Sen_{OFF}HAMP_1AK_{ON} + Sen_{OFF}HAMP_2AK_{ON} + Sen_{ON}HAMP_1AK_{ON} + Sen_{ON}HAMP_2AK_{ON}}{All}$$

$$= \frac{\left(1 + \frac{[Mg^{2+}]}{K_{dOFF}}\right)^2 * (K_{AK} + \alpha_2 K_{HAMP}K_{AK}) + \left(1 + \frac{[Mg^{2+}]}{K_{dON}}\right)^2 * (K_{sen}K_{AK} + \alpha_1\alpha_2 K_{Sen}K_{HAMP}K_{AK})}{\left(1 + \frac{[Mg^{2+}]}{K_{dON}}\right)^2 * (K_{Sen} + K_{sen}K_{AK} + \alpha_1 K_{Sen}K_{HAMP} + \alpha_1\alpha_2 K_{Sen}K_{HAMP}K_{AK}) + \left(1 + \frac{[Mg^{2+}]}{K_{dOFF}}\right)^2 * (1 + K_{AK} + K_{HAMP} + \alpha_2 K_{HAMP}K_{AK})}$$

To ensure equal weights in global fitting, the activity data was scaled by a factor of q = (mean of activity data) / (mean of %crosslink data). The crosslinking data and refactored activity data (Activity / q) were then globally fit to a 3-state allosteric model. Each of 56 datasets (including replicates) was fit by a combination of global and local parameters, described in **Table 2**. Global parameters were shared between replicate datasets as well as datasets of mutations that were functionally similar. A total of 62 parameters (global and local, **Table 2**) were optimized using the python code found in the supplement (phoq_fit_local_global.py), from many rounds of fitting starting with random initial conditions (125,000 independent fits). Error analysis of the best-fit parameters (minimized sum of squares of residuals) was performed through bootstrapping of residuals with replacement to calculate confidence intervals, as well as residual sweep analyses (see below). To create synthetic bootstrapped datasets, we chose residuals at random with replacement and added these residuals to the activity and %crosslink values from the optimum fit. For each synthetic dataset, parameters were re-optimized, starting from initial values taken from the optimum fit. Out of 10,000 generated datasets 3061 fits were determined to have converged. The optimization process was considered converged when the cost function F did not change considerably (dF < ftol * F, with ftol = 1e-8, i.e., convergence criterion 2 from Scipy least_squares). Histograms of these bootstrapped parameter values show the spread in possible

values due to errors in the fit (**Figure 7D** and **Figure 8-figure supplement 1**). Analysis of the bootstrapped parameter distributions showed correlations between the globally fit parameters S and K_{AK} (**Fig. 7-figure supplement 2**).

We also performed a residual sweep analysis to assess the quality of the fit in response to changes in a single parameter value, with all other parameters held fixed. For residual sweep analysis, all but one of the parameters were fixed to their optimum values, and the variable under analysis was swept across its allowed numerical range, after which the sum of squares of residuals was calculated. The sum of squares was then plotted as a function of the parameter's numerical value (**Figure 7D** and **Figure 8-figure supplement 1**). Code to reproduce the fits and plots is given in the comment section at the bottom of the supplement python scripts (phoq_fit_local_global.py, phoq_fit_local_global_ipython.py, and phoq_fit_ci_local_global.py). Scripts to run the fitting on the UCSF Wynton High Performance Computing cluster can also be found in the supplement (phoq_fit.job and phoq_fit_ci.job).

Choice of locally varied parameters: mutations contained entirely within a given domain are allowed to vary the intrinsic equilibrium of that domain only. Mutations within 1 heptad of a domain-domain junction (219/220 for sensor/HAMP, 260/261 for HAMP/autokinase) are also allowed to vary the equilibrium constant of the domain they reside in, as well as the coupling constant between the two domains. Exceptions to this rule include A225F, which was additionally allowed to vary the K_{Sen} parameter, along with K_{HAMP} and α_1 parameters which would normally be varied. Given the poor fit to this mutant, we hypothesized that the disruption of inserting a large Phe sidechain in place of an alanine may propagate into the preceding transmembrane region. Similarly, we allowed K_{AK} to float locally for L254A, N255A and L258A, which resulted in better fits as discussed in main text. Finally, α_2 was allowed to float for

E231A, and E232A, which have been hypothesized in previous work to directly couple to the autokinase domain via a salt-bridge to an arginine residue in the autokinase (68).

Integrative modeling and Molecular dynamics: Rosetta (100), a powerful protein design suite, was employed to produce the initial model of PhoQ. The integrative modeling procedure was used to combine X-ray structures of the PhoQ sensor (PDB id: 3bq8 (101)) and CpxA kinase domain (PDB id: 4biv, (11)), with the atomic model of PhoQ transmembrane domain (102).

A Molecular Dynamics (MD) simulation was carried out to further refine the PhoQ model. The structure was embedded into a phosphatidylcholine (POPC) membrane, solvated in a 17Å padding water box, and neutralized by the addition of NaCl salt at a concentration of 150 mM. No ligands (Mg^{2+}, nucleotides) were present in the simulation. The simulation was performed with the NAMD MD engine (103) and the CHARMM36 force field (104). TIP3P water parameterization was used to describe the water molecules. The periodic electrostatic interactions were computed using particle-mesh Ewald (PME) summation and a grid spacing smaller than 1 Å. Constant temperature of 310 K was imposed with Langevin dynamics, and constant pressure of 1 atm was maintained with a Langevin barostat. During equilibration, the position of the backbone atoms was restrained with harmonic restraints. The system was minimized by 5000 conjugate gradient steps and followed by a 20 ns equilibration. The positional restraints were then replaced with the secondary structure restraints. The molecular dynamics simulation was performed up to 100 ns.

Acknowledgements.

We thank Dr. Mark Goulian for many helpful discussions and sharing E. coli reporter strains.

Funding: We acknowledge research support from a grant from NIH (R35 GM122603).

Table 1- List of mutant parameter fits.

Local parameters whose values remained within 10% of the global fit value are highlighted in bold font and green background. Parameters whose value drifted to one end of the explored parameter range are highlighted in italicized font and orange background. Key: 'TM7' → Gly_7 insertion at 219/220; 'HAMP 4' → Gly_4 insertion at 260/261; 'HAMP 7' / 'H7' → Gly_7 insertion at 260/261; 'SH7' → Gly_7 insertion at 270/271.

Mutation	K_{Sen}	K_{HAMP}	K_{AK}	α_1	α_2	s	K_{dOFF}	K_{dON}
Y60C	9.5 E +02	2.2 E +01	1.4 E -03	5.3 E -03	*1.0 E -08*	7.4 E +02	3.7 E -04	1.6 E -02
Y60C HAMP 4		4.5 E +01			1.0 E +00			
Y60C HAMP 7					1.0 E +00			
Y60C SH7		**2.1 E +01**	7.7 E -04		1.7 E +00			
Y60C TM7				1.0 E +00				
Y40W	1.4 E +03							
S43W	3.8 E +02							
E55A	4.1 E +02							
E55S	1.5 E +03							
V191W	1.2 E +03							
I207A	6.9 E +02			1.1 E -01				
L210A	3.1 E -03			9.1 E +04				
A213W	4.0 E +04			*1.0 E -05*				
S217W		7.1 E -01		7.6 E -01				
S217W + H7					1.0 E +00			
S217W + TM7				1.0 E +00				
I221F		**2.0 E +01**		1.5 E -01				
L224A		1.6 E +01		1.3 E -01				
L224F		6.8 E +01		1.2 E -02				
A225F	**1.0 E +03**	**2.4 E +01**		2.3 E -01				
E232A		1.1 E +02			1.4 E +00			
E232A + H7					1.0 E +00			
E233A		**2.3 E +01**			*1.0 E -08*			
R236A		8.6 E +00						
N240A		1.7 E +01						
R245F		**2.2 E +01**						
L254A			*1.0 E -05*		*1.0 E -08*			
N255A			**1.3 E -03**		4.9 E -01			
N255A + H7					1.0 E +00			
R256A		3.6 E +01			*1.0 E -08*			
L258A			*1.0 E -05*		*1.0 E -08*			
E261F		3.9 E +01			9.9 E -01			
Y265A			4.1 E -04		3.2 E +00			
Y265A + TM7				1.0 E +00				
Y265A + SH7					3.8 E +00			
R269L			3.3 E -04		*1.0 E -08*			

Table 2 - parameters used in fitting

Values in red font indicate parameters fixed to 1 to account for Gly_7 insertion.

Par.	Fit value	lower bound	Upper bound	Fit datasets affected
K_{dON}	1.6 E-02	1.0 E-08	1.0 E+02	ALL
K_{dOFF}	3.7 E-04	1.0 E-08	1.0 E+02	ALL
α_1	5.3 E-03	1.0 E-05	1.0 E+05	Y60C_Gly_7 270/271, Y60C_Gly_7 260/261, Y60C_Gly_4 260/261, Y60C, Y40W, Y265A_Gly_7 270/271, Y265A, V191W, S43W, R269L, R256A, R245F, R236A, N255A Gly7 260/261, N255A, N240A, L258A, L254A, E55S, E55A, E261F, E233A, E232A_Gly_7 260/261, E232A
α_2	1.0 E-08	1.0 E-08	1.0 E+02	Y60C_Gly_7 219/220, Y60C, Y40W, V191W, S43W, S217_Gly_7 219/220, S217W, R245F, R236A, N240A, L224F, L224A, L210A, I221F, I207A, E55S, E55A, A225F, A213W
K_{Sen}	9.5 E+02	1.0 E-05	1.0 E+05	Y60C_Gly_7 219/220, Y60C_Gly_7 270/271, Y60C_Gly_7 260/261, Y60C_Gly_4 260/261, Y60C, Y265A_Gly_7 270/271, Y265A, S217W_Gly_7 219/220, S217W_Gly_7 260/261, S217W, R269L, R256A, R245F, R236A, N255A_Gly_7 260/261, N255A, N240A, L258A, L254A, L224F, L224A, L210A, I221F, I207A, E261F, E233A, E232A_Gly_7 260/261, E232A
K_{HAMP}	2.2 E+01	1.0 E-05	1.0 E+05	Y60C_Gly_7 219/220, Y60C, Y40W, Y265A_Gly_7 219/220, Y265A_Gly_7 270/271, Y265A, V191W, S43W, R269L, E55S, E55A, A213W
K_{AK}	1.4 E-03	1.0 E-05	1.0 E+05	Y60C_Gly_7 219/220, Y60C_Gly_7 260/261, Y60C_Gly_4 260/261, Y60C, Y40W, V191W, S43W, S217W_Gly_7 219/220, S217W_Gly_7 260/261, S217W, R256A, R245F, R236A, N255A_Gly_7 260/261, N255A, N240A, L258A, L254A, L224F, L224A, L210A, I221F, I207A, E55S, E55A, E261F, E233A, E232A_Gly_7 260/261, E232A, A225F, A213W
S	7.4 E+02	1.0 E-05	1.0 E+05	ALL
K_{Sen}	1.4 E+03	1.0 E-05	1.0 E+05	Y40W
K_{Sen}	3.8 E+02	1.0 E-05	1.0 E+05	S43W
K_{Sen}	4.1 E+02	1.0 E-05	1.0 E+05	E55A
K_{Sen}	1.5 E+03	1.0 E-05	1.0 E+05	E55S
K_{Sen}	1.2 E+03	1.0 E-05	1.0 E+05	V191W
K_{Sen}	6.9 E+02	1.0 E-05	1.0 E+05	I207A
α_1	1.1 E-01	1.0 E-05	1.0 E+05	I207A
K_{Sen}	3.1 E-03	1.0 E-05	1.0 E+05	L210A
α_1	9.1 E+04	1.0 E-05	1.0 E+05	L210A
α_1	1.0 E-05	1.0 E-05	1.0 E+05	A213W
K_{Sen}	4.0 E+04	1.0 E-05	1.0 E+05	A213W
K_{HAMP}	7.1 E-01	1.0 E-05	1.0 E+05	S217W_Gly_7 219/220, S217W_Gly_7 260/261, S217W
α_1	7.6 E-01	1.0 E-05	1.0 E+05	S217W_Gly_7 260/261, S217W
K_{HAMP}	2.0 E+01	1.0 E-05	1.0 E+05	I221F

α_1	1.5 E-01	1.0 E-05	1.0 E+05	I221F
K_{HAMP}	1.6 E+01	1.0 E-05	1.0 E+05	L224A
α_1	1.3 E-01	1.0 E-05	1.0 E+05	L224A
Par.	**Fit value**	**lower bound**	**Upper bound**	**Fit datasets affected**
K_{HAMP}	6.8 E+01	1.0 E-05	1.0 E+05	L224F
α_1	1.2 E-02	1.0 E-05	1.0 E+05	L224F
K_{HAMP}	2.4 E+01	1.0 E-05	1.0 E+05	A225F
α_1	2.3 E-01	1.0 E-05	1.0 E+05	A225F
K_{Sen}	1.0 E+03	1.0 E-05	1.0 E+05	A225F
K_{HAMP}	1.1 E+02	1.0 E-05	1.0 E+05	E232A_Gly_7 260/261, E232A
α_2	1.4 E+00	1.0 E-08	1.0 E+02	E232A
K_{HAMP}	2.4 E+01	1.0 E-05	1.0 E+05	E233A
α_2	1.0 E-08	1.0 E-08	1.0 E+02	E233A
K_{HAMP}	8.6 E+00	1.0 E-05	1.0 E+05	R236A
K_{HAMP}	1.7 E+01	1.0 E-05	1.0 E+05	N240A
K_{HAMP}	2.2 E+01	1.0 E-05	1.0 E+05	R245F
K_{AK}	1.0 E-05	1.0 E-05	1.0 E+05	L254A
α_2	1.0 E-08	1.0 E-08	1.0 E+02	L254A
K_{AK}	1.3 E-03	1.0 E-05	1.0 E+05	N255A_Gly_7 260/261, N255A
α_2	4.9 E-01	1.0 E-08	1.0 E+02	N255A
K_{HAMP}	3.6 E+01	1.0 E-05	1.0 E+05	R256A
α_2	1.0 E-08	1.0 E-08	1.0 E+02	R256A
K_{AK}	1.0 E-05	1.0 E-05	1.0 E+05	L258A
α_2	1.0 E-08	1.0 E-08	1.0 E+02	L258A
K_{HAMP}	3.9 E+01	1.0 E-05	1.0 E+05	E261F
α_2	9.9 E-01	1.0 E-08	1.0 E+02	E261F
K_{AK}	4.1 E-04	1.0 E-05	1.0 E+05	Y265A_Gly_7 219/220, Y265A_Gly_7 270/271, Y265A
α_2	3.2 E+00	1.0 E-08	1.0 E+02	Y265A_Gly_7 219/220, Y265A
K_{AK}	3.3 E-03	1.0 E-05	1.0 E+05	R269L
α_2	1.0 E-08	1.0 E-08	1.0 E+02	R269L
K_{HAMP}	4.5 E+01	1.0 E-05	1.0 E+05	Y60C_Gly_7 260/261, Y60C_Gly_4 260/261
α_2	1.0 E+00			Y60C_Gly_7 260;261, Y60C_Gly_4 260/261
α_2	1.0 E+00			S217W_Gly_7 260/261
α_2	1.0 E+00			E232A_Gly_7 260/261
α_2	1.0 E+00			N255A_Gly_7 260/261
α_1	1.0 E+00			Y60C_Gly_7 219/220
α_1	1.0 E+00			S217W_Gly_7 219/220
α_1	1.0 E+00			Y265A_Gly_7 219/220
K_{HAMP}	2.1 E+01	1.0 E-05	1.0 E+05	Y60C_Gly_7 270/271
K_{AK}	7.8 E-04	1.0 E-05	1.0 E+05	Y60C_Gly_7 270/271
α_2	1.7 E+00	1.0 E-08	1.0 E+02	Y60C_Gly_7 270/271
α_2	3.8 E+00	1.0 E-08	1.0 E+02	Y265A_Gly_7 270/271

896

References

1. A. M. Stock, V. L. Robinson, P. N. Goudreau, Two-component signal transduction. *Annu. Rev. Biochem.* **69**, 183–215 (2000).

2. E. A. Groisman, C. Mouslim, Sensing by bacterial regulatory systems in host and non-host environments. *Nat. Rev. Microbiol.* **4**, 705–709 (2006).

3. K. Nishino, T. Honda, A. Yamaguchi, Genome-wide analyses of Escherichia coli gene expression responsive to the BaeSR two-component regulatory system. *J. Bacteriol.* **187**, 1763–1772 (2005).

4. H. Hirakawa, K. Nishino, T. Hirata, A. Yamaguchi, Comprehensive studies of drug resistance mediated by overexpression of response regulators of two-component signal transduction systems in Escherichia coli. *J. Bacteriol.* **185**, 1851–1856 (2003).

5. V. Nizet, Antimicrobial peptide resistance mechanisms of human bacterial pathogens. *Curr. Issues Mol. Biol.* **8**, 11–26 (2006).

6. L. Thomas, L. Cook, Two-Component Signal Transduction Systems in the Human Pathogen Streptococcus agalactiae. *Infect. Immun.* **88** (2020).

7. A. Delauné, *et al.*, The WalKR system controls major staphylococcal virulence genes and is involved in triggering the host inflammatory response. *Infect. Immun.* **80**, 3438–3453 (2012).

8. H. U. Ferris, M. Coles, A. N. Lupas, M. D. Hartmann, Crystallographic snapshot of the Escherichia coli EnvZ histidine kinase in an active conformation. *J. Struct. Biol.* **186**, 376–379 (2014).

9. G. Rivera-Cancel, W. Ko, D. R. Tomchick, F. Correa, K. H. Gardner, Full-length structure of a monomeric histidine kinase reveals basis for sensory regulation. *Proc. Natl. Acad. Sci. U. S. A.* **111**, 17839–17844 (2014).

10. C. Wang, *et al.*, Mechanistic insights revealed by the crystal structure of a histidine kinase with signal transducer and sensor domains. *PLoS Biol.* **11**, e1001493 (2013).

11. A. E. Mechaly, N. Sassoon, J.-M. Betton, P. M. Alzari, Segmental helical motions and dynamical asymmetry modulate histidine kinase autophosphorylation. *PLoS Biol.* **12**, e1001776 (2014).

12. A. E. Mechaly, *et al.*, Structural Coupling between Autokinase and Phosphotransferase Reactions in a Bacterial Histidine Kinase. *Struct. Lond. Engl. 1993* **25**, 939-944.e3 (2017).

13. P. Casino, V. Rubio, A. Marina, Structural insight into partner specificity and phosphoryl transfer in two-component signal transduction. *Cell* **139**, 325–336 (2009).

14. D. Albanesi, *et al.*, Structural plasticity and catalysis regulation of a thermosensor histidine kinase. *Proc. Natl. Acad. Sci. U. S. A.* **106**, 16185–16190 (2009).

15. F. Jacob-Dubuisson, A. Mechaly, J.-M. Betton, R. Antoine, Structural insights into the signalling mechanisms of two-component systems. *Nat. Rev. Microbiol.* **16**, 585–593 (2018).

16. T. Krell, *et al.*, Bacterial sensor kinases: diversity in the recognition of environmental signals. *Annu. Rev. Microbiol.* **64**, 539–559 (2010).

17. M. P. Bhate, K. S. Molnar, M. Goulian, W. F. DeGrado, Signal transduction in histidine kinases: insights from new structures. *Struct. Lond. Engl. 1993* **23**, 981–994 (2015).

18. S. I. Miller, A. M. Kukral, J. J. Mekalanos, A two-component regulatory system (phoP phoQ) controls Salmonella typhimurium virulence. *Proc. Natl. Acad. Sci. U. S. A.* **86**, 5054–5058 (1989).

19. E. García Véscovi, F. C. Soncini, E. A. Groisman, Mg2+ as an extracellular signal: environmental regulation of Salmonella virulence. *Cell* **84**, 165–174 (1996).

20. F. C. Soncini, E. García Véscovi, F. Solomon, E. A. Groisman, Molecular basis of the magnesium deprivation response in Salmonella typhimurium: identification of PhoP-regulated genes. *J. Bacteriol.* **178**, 5092–5099 (1996).

21. M. W. Bader, *et al.*, Recognition of antimicrobial peptides by a bacterial sensor kinase. *Cell* **122**, 461–472 (2005).

22. R. E. W. Hancock, J. B. McPhee, Salmonella's sensor for host defense molecules. *Cell* **122**, 320–322 (2005).

23. E. A. Groisman, E. Chiao, C. J. Lipps, F. Heffron, Salmonella typhimurium phoP virulence gene is a transcriptional regulator. *Proc. Natl. Acad. Sci. U. S. A.* **86**, 7077–7081 (1989).

24. P. I. Fields, E. A. Groisman, F. Heffron, A Salmonella locus that controls resistance to microbicidal proteins from phagocytic cells. *Science* **243**, 1059–1062 (1989).

25. I. Behlau, S. I. Miller, A PhoP-repressed gene promotes Salmonella typhimurium invasion of epithelial cells. *J. Bacteriol.* **175**, 4475–4484 (1993).

26. W. J. Belden, S. I. Miller, Further characterization of the PhoP regulon: identification of new PhoP-activated virulence loci. *Infect. Immun.* **62**, 5095–5101 (1994).

27. J. S. Gunn, S. I. Miller, PhoP-PhoQ activates transcription of pmrAB, encoding a two-component regulatory system involved in Salmonella typhimurium antimicrobial peptide resistance. *J. Bacteriol.* **178**, 6857–6864 (1996).

28. L. Guo, *et al.*, Regulation of lipid A modifications by Salmonella typhimurium virulence genes phoP-phoQ. *Science* **276**, 250–253 (1997).

29. B. L. Bearson, L. Wilson, J. W. Foster, A low pH-inducible, PhoPQ-dependent acid tolerance response protects Salmonella typhimurium against inorganic acid stress. *J. Bacteriol.* **180**, 2409–2417 (1998).

30. L. Guo, *et al.*, Lipid A acylation and bacterial resistance against vertebrate antimicrobial peptides. *Cell* **95**, 189–198 (1998).

31. P. Adams, *et al.*, Proteomic detection of PhoPQ- and acid-mediated repression of Salmonella motility. *Proteomics* **1**, 597–607 (2001).

32. M. W. Bader, *et al.*, Regulation of Salmonella typhimurium virulence gene expression by cationic antimicrobial peptides. *Mol. Microbiol.* **50**, 219–230 (2003).

33. Z. D. Dalebroux, S. Matamouros, D. Whittington, R. E. Bishop, S. I. Miller, PhoPQ regulates acidic glycerophospholipid content of the Salmonella Typhimurium outer membrane. *Proc. Natl. Acad. Sci. U. S. A.* **111**, 1963–1968 (2014).

34. L. R. Prost, *et al.*, Activation of the bacterial sensor kinase PhoQ by acidic pH. *Mol. Cell* **26**, 165–174 (2007).

35. J. Choi, E. A. Groisman, Activation of master virulence regulator PhoP in acidic pH requires the Salmonella-specific protein UgtL. *Sci. Signal.* **10** (2017).

36. J. Yuan, F. Jin, T. Glatter, V. Sourjik, Osmosensing by the bacterial PhoQ/PhoP two-component system. *Proc. Natl. Acad. Sci. U. S. A.* **114**, E10792–E10798 (2017).

37. U. S. Cho, *et al.*, Metal bridges between the PhoQ sensor domain and the membrane regulate transmembrane signaling. *J. Mol. Biol.* **356**, 1193–1206 (2006).

38. S. Chamnongpol, M. Cromie, E. A. Groisman, Mg2+ sensing by the Mg2+ sensor PhoQ of Salmonella enterica. *J. Mol. Biol.* **325**, 795–807 (2003).

39. K. S. Molnar, *et al.*, Cys-scanning disulfide crosslinking and bayesian modeling probe the transmembrane signaling mechanism of the histidine kinase, PhoQ. *Struct. Lond. Engl. 1993* **22**, 1239–1251 (2014).

40. H. Kadokura, J. Beckwith, Mechanisms of oxidative protein folding in the bacterial cell envelope. *Antioxid. Redox Signal.* **13**, 1231–1246 (2010).

41. T. Miyashiro, M. Goulian, Stimulus-dependent differential regulation in the Escherichia coli PhoQ PhoP system. *Proc. Natl. Acad. Sci. U. S. A.* **104**, 16305–16310 (2007).

42. J. J. Falke, G. L. Hazelbauer, Transmembrane signaling in bacterial chemoreceptors. *Trends Biochem. Sci.* **26**, 257–265 (2001).

43. K. E. Swain, J. J. Falke, Structure of the conserved HAMP domain in an intact, membrane-bound chemoreceptor: a disulfide mapping study. *Biochemistry* **46**, 13684–13695 (2007).

44. M. V. Airola, *et al.*, HAMP domain conformers that propagate opposite signals in bacterial chemoreceptors. *PLoS Biol.* **11**, e1001479 (2013).

45. H. U. Ferris, *et al.*, The mechanisms of HAMP-mediated signaling in transmembrane receptors. *Struct. Lond. Engl. 1993* **19**, 378–385 (2011).

46. M. Hulko, *et al.*, The HAMP domain structure implies helix rotation in transmembrane signaling. *Cell* **126**, 929–940 (2006).

47. S. Bi, F. Jin, V. Sourjik, Inverted signaling by bacterial chemotaxis receptors. *Nat. Commun.* **9**, 2927 (2018).

48. R. R. Draheim, A. F. Bormans, R. Lai, M. D. Manson, Tryptophan residues flanking the second transmembrane helix (TM2) set the signaling state of the Tar chemoreceptor. *Biochemistry* **44**, 1268–1277 (2005).

49. C. E. Lehning, J. B. Heidelberger, J. Reinhard, M. H. H. Nørholm, R. R. Draheim, A Modular High-Throughput In Vivo Screening Platform Based on Chimeric Bacterial Receptors. *ACS Synth. Biol.* **6**, 1315–1326 (2017).

50. M. E. Inda, R. G. Oliveira, D. de Mendoza, L. E. Cybulski, The Single Transmembrane Segment of Minimal Sensor DesK Senses Temperature via a Membrane-Thickness Caliper. *J. Bacteriol.* **198**, 2945–2954 (2016).

51. C. Monzel, G. Unden, Transmembrane signaling in the sensor kinase DcuS of Escherichia coli: A long-range piston-type displacement of transmembrane helix 2. *Proc. Natl. Acad. Sci. U. S. A.* **112**, 11042–11047 (2015).

52. R. Yusuf, R. R. Draheim, Employing aromatic tuning to modulate output from two-component signaling circuits. *J. Biol. Eng.* **9**, 7 (2015).

53. R. Yusuf, R. J. Lawrence, L. V. Eke, R. R. Draheim, Tuning Chemoreceptor Signaling by Positioning Aromatic Residues at the Lipid-Aqueous Interface. *Methods Mol. Biol. Clifton NJ* **1729**, 147–158 (2018).

54. C. A. Adase, R. R. Draheim, G. Rueda, R. Desai, M. D. Manson, Residues at the cytoplasmic end of transmembrane helix 2 determine the signal output of the TarEc chemoreceptor. *Biochemistry* **52**, 2729–2738 (2013).

55. R. W. Scott, W. F. DeGrado, G. N. Tew, De novo designed synthetic mimics of antimicrobial peptides. *Curr. Opin. Biotechnol.* **19**, 620–627 (2008).

56. B. Mensa, *et al.*, Antibacterial mechanism of action of arylamide foldamers. *Antimicrob. Agents Chemother.* **55**, 5043–5053 (2011).

57. R. Keller, *et al.*, The Escherichia coli Envelope Stress Sensor CpxA Responds to Changes in Lipid Bilayer Properties. *Biochemistry* **54**, 3670–3676 (2015).

58. E. Batchelor, D. Walthers, L. J. Kenney, M. Goulian, The Escherichia coli CpxA-CpxR envelope stress response system regulates expression of the porins ompF and ompC. *J. Bacteriol.* **187**, 5723–5731 (2005).

59. P. N. Danese, T. J. Silhavy, The sigma(E) and the Cpx signal transduction systems control the synthesis of periplasmic protein-folding enzymes in Escherichia coli. *Genes Dev.* **11**, 1183–1193 (1997).

60. X. Zhou, *et al.*, Structural basis for two-component system inhibition and pilus sensing by the auxiliary CpxP protein. *J. Biol. Chem.* **286**, 9805–9814 (2011).

61. S. K. D. Leblanc, C. W. Oates, T. L. Raivio, Characterization of the induction and cellular role of the BaeSR two-component envelope stress response of Escherichia coli. *J. Bacteriol.* **193**, 3367–3375 (2011).

62. I. C. Clark, *et al.*, Protein design-scapes generated by microfluidic DNA assembly elucidate domain coupling in the bacterial histidine kinase CpxA. *Proc. Natl. Acad. Sci. U. S. A.* **118**, e2017719118 (2021).

63. J. E. Gestwicki, L. E. Strong, L. L. Kiessling, Tuning chemotactic responses with synthetic multivalent ligands. *Chem. Biol.* **7**, 583–591 (2000).

64. C. D. Waldburger, R. T. Sauer, Signal detection by the PhoQ sensor-transmitter. Characterization of the sensor domain and a response-impaired mutant that identifies ligand-binding determinants. *J. Biol. Chem.* **271**, 26630–26636 (1996).

65. P. Fernández, *et al.*, Transmembrane Prolines Mediate Signal Sensing and Decoding in Bacillus subtilis DesK Histidine Kinase. *mBio* **10** (2019).

66. L. C. Wang, L. K. Morgan, P. Godakumbura, L. J. Kenney, G. S. Anand, The inner membrane histidine kinase EnvZ senses osmolality via helix-coil transitions in the cytoplasm. *EMBO J.* **34**, 2481 (2015).

67. A. Koh, M. J. Gibbon, M. W. Van der Kamp, C. R. Pudney, S. Gebhard, Conformation control of the histidine kinase BceS of Bacillus subtilis by its cognate ABC-transporter facilitates need-based activation of antibiotic resistance. *Mol. Microbiol.* **115**, 157–174 (2021).

68. S. Matamouros, K. R. Hager, S. I. Miller, HAMP Domain Rotation and Tilting Movements Associated with Signal Transduction in the PhoQ Sensor Kinase. *mBio* **6**, e00616-00615 (2015).

69. A. Baruah, B. Lindsey, Y. Zhu, M. M. Nakano, Mutational analysis of the signal-sensing domain of ResE histidine kinase from Bacillus subtilis. *J. Bacteriol.* **186**, 1694–1704 (2004).

70. Y. Eguchi, R. Utsumi, Alkali metals in addition to acidic pH activate the EvgS histidine kinase sensor in Escherichia coli. *J. Bacteriol.* **196**, 3140–3149 (2014).

71. R. Gao, D. G. Lynn, Environmental pH sensing: resolving the VirA/VirG two-component system inputs for Agrobacterium pathogenesis. *J. Bacteriol.* **187**, 2182–2189 (2005).

72. K. Yoshitani, *et al.*, Identification of an internal cavity in the PhoQ sensor domain for PhoQ activity and SafA-mediated control. *Biosci. Biotechnol. Biochem.* **83**, 684–694 (2019).

73. K. G. Hicks, *et al.*, Acidic pH and divalent cation sensing by PhoQ are dispensable for systemic salmonellae virulence. *eLife* **4**, e06792 (2015).

74. S. J. Edelstein, J. P. Changeux, Allosteric proteins after thirty years: the binding and state functions of the neuronal alpha 7 nicotinic acetylcholine receptors. *Experientia* **52**, 1083–1090 (1996).

75. J. S. Smith, R. J. Lefkowitz, S. Rajagopal, Biased signalling: from simple switches to allosteric microprocessors. *Nat. Rev. Drug Discov.* **17**, 243–260 (2018).

76. J.-P. Changeux, S. J. Edelstein, Allosteric mechanisms of signal transduction. *Science* **308**, 1424–1428 (2005).

77. A. De Lean, J. M. Stadel, R. J. Lefkowitz, A ternary complex model explains the agonist-specific binding properties of the adenylate cyclase-coupled beta-adrenergic receptor. *J. Biol. Chem.* **255**, 7108–7117 (1980).

78. O. Ashenberg, K. Rozen-Gagnon, M. T. Laub, A. E. Keating, Determinants of homodimerization specificity in histidine kinases. *J. Mol. Biol.* **413**, 222–235 (2011).

79. A. I. Podgornaia, P. Casino, A. Marina, M. T. Laub, Structural basis of a rationally rewired protein-protein interface critical to bacterial signaling. *Struct. Lond. Engl. 1993* **21**, 1636–1647 (2013).

80. J. M. Skerker, *et al.*, Rewiring the specificity of two-component signal transduction systems. *Cell* **133**, 1043–1054 (2008).

81. A. Buschiazzo, F. Trajtenberg, Two-Component Sensing and Regulation: How Do Histidine Kinases Talk with Response Regulators at the Molecular Level? *Annu. Rev. Microbiol.* **73**, 507–528 (2019).

82. N. Ohta, A. Newton, The core dimerization domains of histidine kinases contain recognition specificity for the cognate response regulator. *J. Bacteriol.* **185**, 4424–4431 (2003).

83. M. E. Salazar, M. T. Laub, Temporal and evolutionary dynamics of two-component signaling pathways. *Curr. Opin. Microbiol.* **24**, 7–14 (2015).

84. V. Anantharaman, S. Balaji, L. Aravind, The signaling helix: a common functional theme in diverse signaling proteins. *Biol. Direct* **1**, 25 (2006).

85. N. W. Schmidt, G. Grigoryan, W. F. DeGrado, The accommodation index measures the perturbation associated with insertions and deletions in coiled-coils: Application to understand signaling in histidine kinases. *Protein Sci. Publ. Protein Soc.* **26**, 414–435 (2017).

86. M. Motz, K. Jung, The role of polyproline motifs in the histidine kinase EnvZ. *PloS One* **13**, e0199782 (2018).

87. N. Akkaladevi, F. Bunyak, D. Stalla, T. A. White, G. L. Hazelbauer, Flexible Hinges in Bacterial Chemoreceptors. *J. Bacteriol.* **200** (2018).

88. M. Inouye, Signaling by transmembrane proteins shifts gears. *Cell* **126**, 829–831 (2006).

89. S. A. Chervitz, J. J. Falke, Molecular mechanism of transmembrane signaling by the aspartate receptor: a model. *Proc. Natl. Acad. Sci. U. S. A.* **93**, 2545–2550 (1996).

90. J. J. Falke, A. H. Erbse, The piston rises again. *Struct. Lond. Engl. 1993* **17**, 1149–1151 (2009).

91. M. V. Milburn, *et al.*, Three-dimensional structures of the ligand-binding domain of the bacterial aspartate receptor with and without a ligand. *Science* **254**, 1342–1347 (1991).

92. E. C. Lowe, A. Baslé, M. Czjzek, S. J. Firbank, D. N. Bolam, A scissor blade-like closing mechanism implicated in transmembrane signaling in a Bacteroides hybrid two-component system. *Proc. Natl. Acad. Sci. U. S. A.* **109**, 7298–7303 (2012).

93. M. V. Airola, K. J. Watts, A. M. Bilwes, B. R. Crane, Structure of concatenated HAMP domains provides a mechanism for signal transduction. *Struct. Lond. Engl. 1993* **18**, 436–448 (2010).

94. K. E. Swain, M. A. Gonzalez, J. J. Falke, Engineered socket study of signaling through a four-helix bundle: evidence for a yin-yang mechanism in the kinase control module of the aspartate receptor. *Biochemistry* **48**, 9266–9277 (2009).

95. J. S. Parkinson, Signaling mechanisms of HAMP domains in chemoreceptors and sensor kinases. *Annu. Rev. Microbiol.* **64**, 101–122 (2010).

96. V. Stewart, The HAMP signal-conversion domain: static two-state or dynamic three-state? *Mol. Microbiol.* **91**, 853–857 (2014).

97. I. Gushchin, *et al.*, Mechanism of transmembrane signaling by sensor histidine kinases. *Science* **356** (2017).

98. N. Sukomon, J. Widom, P. P. Borbat, J. H. Freed, B. R. Crane, Stability and Conformation of a Chemoreceptor HAMP Domain Chimera Correlates with Signaling Properties. *Biophys. J.* **112**, 1383–1395 (2017).

99. D. G. Gibson, *et al.*, Enzymatic assembly of DNA molecules up to several hundred kilobases. *Nat. Methods* **6**, 343–345 (2009).

100. A. Leaver-Fay, *et al.*, ROSETTA3: an object-oriented software suite for the simulation and design of macromolecules. *Methods Enzymol.* **487**, 545–574 (2011).

101. J. Cheung, C. A. Bingman, M. Reyngold, W. A. Hendrickson, C. D. Waldburger, Crystal structure of a functional dimer of the PhoQ sensor domain. *J. Biol. Chem.* **283**, 13762–13770 (2008).

102. T. Lemmin, C. S. Soto, G. Clinthorne, W. F. DeGrado, M. Dal Peraro, Assembly of the transmembrane domain of E. coli PhoQ histidine kinase: implications for signal transduction from molecular simulations. *PLoS Comput. Biol.* **9**, e1002878 (2013).

103. J. C. Phillips, *et al.*, Scalable molecular dynamics on CPU and GPU architectures with NAMD. *J. Chem. Phys.* **153**, 044130 (2020).

104. J. Huang, A. D. MacKerell, CHARMM36 all-atom additive protein force field: validation based on comparison to NMR data. *J. Comput. Chem.* **34**, 2135–2145 (2013).